NAVAL POSTGRADUATE SCHOOL

MONTEREY, CALIFORNIA

THESIS

REMOTE DETECTION OF CLOUD BASE HEIGHTS USING CLOUDSAT AND CALIPSO

by

Elizabeth Welliver

March 2009

Thesis Advisor: Philip A. Durkee
Second Reader: Qing Wang

Approved for public release; distribution is unlimited.

THIS PAGE INTENTIONALLY LEFT BLANK

REPORT DOCUMENTATION PAGE		Form Approved OMB No. 0704-0188

Public reporting burden for this collection of information is estimated to average 1 hour per response, including the time for reviewing instruction, searching existing data sources, gathering and maintaining the data needed, and completing and reviewing the collection of information. Send comments regarding this burden estimate or any other aspect of this collection of information, including suggestions for reducing this burden, to Washington headquarters Services, Directorate for Information Operations and Reports, 1215 Jefferson Davis Highway, Suite 1204, Arlington, VA 22202-4302, and to the Office of Management and Budget, Paperwork Reduction Project (0704-0188) Washington DC 20503.

1. AGENCY USE ONLY *(Leave blank)*	2. REPORT DATE March 2009	3. REPORT TYPE AND DATES COVERED Master's Thesis	
4. TITLE AND SUBTITLE Remote Detection of Cloud Base Heights Using CloudSat and CALIPSO		5. FUNDING NUMBERS	
6. AUTHOR(S) Elizabeth A. Welliver			
7. PERFORMING ORGANIZATION NAME(S) AND ADDRESS(ES) Naval Postgraduate School Monterey, CA 93943-5000		8. PERFORMING ORGANIZATION REPORT NUMBER	
9. SPONSORING /MONITORING AGENCY NAME(S) AND ADDRESS(ES) N/A		10. SPONSORING/MONITORING AGENCY REPORT NUMBER	

11. SUPPLEMENTARY NOTES The views expressed in this thesis are those of the author and do not reflect the official policy or position of the Department of Defense or the U.S. Government.

12a. DISTRIBUTION / AVAILABILITY STATEMENT Approved for public release; distribution is unlimited.	12b. DISTRIBUTION CODE

13. ABSTRACT (maximum 200 words)

This thesis study focuses on the evaluation of cloud base height from a pair of space-based remote sensing systems. The first satellite, CloudSat, is a 94-GHz cloud profiling radar (CPR) utilizing a wavelength capable of penetrating thick hydrometeor layers. The second satellite, the Cloud-Aerosol Lidar and Infrared Pathfinder Satellite Observations (CALIPSO) satellite, is an active lidar designed to detect optically thin hydrometeor layers. The 2B-GEOPROF-Lidar product combines data from these two synergistic observing platforms to provide a complete profile of the vertical structure of clouds in the atmosphere. For this research, 2B-GEOPROF-Lidar cloud base height measurements were validated against cloud base height measurements from a combined suite of ground-based sensors at four Department of Energy (DOE) Atmospheric Radiation Measurement (ARM) sites. Cloud base height measurements validated within 480 meters, the vertical resolution of the CPR, were deemed accurate assessments. Differences in cloud base height exceeding 720 meters were labeled as significant outliers. Significant outliers were further investigated to find trends in radar reflectivity and cloud mask data from CloudSat and total attenuated backscatter from CALIPSO. The combined CloudSat / CALIPSO cloud base assessment proved accurate in 73% of the cases studied.

14. SUBJECT TERMS CloudSat, CALIPSO, cloud base height, remote sensing			15. NUMBER OF PAGES 63
			16. PRICE CODE
17. SECURITY CLASSIFICATION OF REPORT Unclassified	18. SECURITY CLASSIFICATION OF THIS PAGE Unclassified	19. SECURITY CLASSIFICATION OF ABSTRACT Unclassified	20. LIMITATION OF ABSTRACT UU

NSN 7540-01-280-5500

Standard Form 298 (Rev. 2-89)
Prescribed by ANSI Std. 239-18

THIS PAGE INTENTIONALLY LEFT BLANK

REMOTE DETECTION OF CLOUD BASE HEIGHTS USING CLOUDSAT AND CALIPSO

Elizabeth A. Welliver
Captain, United States Air Force
B.S., United States Air Force Academy, 2002

Submitted in partial fulfillment of the
requirements for the degree of

MASTER OF SCIENCE IN METEOROLOGY

from the

**NAVAL POSTGRADUATE SCHOOL
March 2009**

Author: Elizabeth A. Welliver

Approved by: Philip A. Durkee
                    Thesis Advisor

                    Qing Wang
                    Second Reader

                    Philip A. Durkee
                    Chairman, Department of Meteorology

THIS PAGE INTENTIONALLY LEFT BLANK

ABSTRACT

This thesis study focuses on the evaluation of cloud base height from a pair of space-based remote sensing systems. The first satellite, CloudSat, is a 94-GHz cloud profiling radar (CPR) utilizing a wavelength capable of penetrating thick hydrometeor layers. The second satellite, the Cloud-Aerosol Lidar and Infrared Pathfinder Satellite Observations (CALIPSO) satellite, is an active lidar designed to detect optically thin hydrometeor layers. The 2B-GEOPROF-Lidar product combines data from these two synergistic observing platforms to provide a complete profile of the vertical structure of clouds in the atmosphere. For this research, 2B-GEOPROF-Lidar cloud base height measurements were validated against cloud base height measurements from a combined suite of ground-based sensors at four Department of Energy (DOE) Atmospheric Radiation Measurement (ARM) sites. Cloud base height measurements validated within 480 meters, the vertical resolution of the CPR, were deemed accurate assessments. Differences in cloud base height exceeding 720 meters were labeled as significant outliers. Significant outliers were further investigated to find trends in radar reflectivity and cloud mask data from CloudSat and total attenuated backscatter from CALIPSO. The combined CloudSat / CALIPSO cloud base assessment proved accurate in 73% of the cases studied.

THIS PAGE INTENTIONALLY LEFT BLANK

TABLE OF CONTENTS

THIS PAGE INTENTIONALLY LEFT BLANK

LIST OF FIGURES

LIST OF TABLES

THIS PAGE INTENTIONALLY LEFT BLANK

ACKNOWLEDGMENTS

THIS PAGE INTENTIONALLY LEFT BLANK

I.   INTRODUCTION

A.   THE CHALLENGE OF REMOTELY DETERMINING CLOUD BASE HEIGHT

The remote detection of cloud base heights is a critical topic of interest for the Department of Defense (DoD). While cloud base heights are freely available for points with a human observer present or equipped with automated observation sensors, these heights are virtually impossible to determine in remote locations. Low ceilings can severely impact operations ranging from aircraft take-off and landings to reconnaissance and surveillance missions to close air support and air assault missions. Due to the data sparseness in the highly remote, yet mission-critical operating areas of Afghanistan and Southeast Asia, accurate cloud base height analysis is necessary for both safe and successful operations. Even large areas of the United States lack consistently available and reliable ground observations, making training, weapons testing, and search and rescues missions a challenge. Accurate cloud base height assessment for these austere operating environments has the potential to drastically improve mission accomplishment.

Despite significant advances in recent years in cloud detection, identification, and modeling schemes, the correct assessment of cloud base heights remains a significant deficiency in global cloud analysis and forecasting, especially in remote areas. Previous research utilizing space-based remote sensing systems to obtain cloud base height failed to yield conclusive improvement in remote locations, primarily because the satellite sensors employed wavelengths that were not able to penetrate the entire depth of the cloud (Lhermitte 1988, Forsythe et al. 2000). However, with the April 2006 launch of the CloudSat 94-GHz Cloud Profiling Radar, and the Cloud-Aerosol Lidar and Infrared Pathfinder Observation (CALIPSO) satellite, the remote sensing of the vertical distribution and structure of hydrometeors in the atmosphere is now a reality. Specifically, accurate measurements of cloud base height are now possible from these space-based platforms, thus providing a realistic assessment of cloud base height in remote, unobserved locations.

B.   PREVIOUS RESEARCH AND METHODS

Until recently, space-based cloud base height assessments have generally relied on the interpolation of available satellite imagery.   For example, GOES-8 satellite-derived cloud classification combined with surface observations of cloud base height yielded positive results when surface observations reported broken or greater cloud decks (Forsythe et al. 2000). The horizontal interpolation of surface observations combined with the bispectral satellite imagery showed improvement over previous methods that relied solely on distance-weighted interpolation of surface cloud observations. However, this method struggled to accurately identify the height of mid- and high-level clouds, and fell victim to the tendency of human surface observers to report heights at "meteorologically significant" levels, thus failing to observe the exact height.

The development of millimeter wavelength radars significantly improved hydrometeor detection in clouds and precipitation over previously used centimeter wavelength radars (Lhermitte 1988). Lhermitte demonstrated that a vertically pointing 94-GHz radar provided improved observation of low-altitude, low-reflectivity clouds over the commonly used 35-GHz wavelengths. Attenuation of 94-GHz radiation is caused either by the absorption or scattering of radiative energy by hydrometeors. Through analysis of the backscattered energy by cloud particles within the Rayleigh scattering regime and the associated attenuation of radar reflectivity, accurate cloud layer detection is possible.

A cloud detection algorithm utilizing the 94-GHz frequency can provide objective estimates of cloud boundaries, both top and bottom, as well as multiple cloud layers (Clothiaux 1995). The algorithm focuses on detecting significant power signals received at the radar. The criterion for significant detection is:

$$\overline{P_r(mW)} = \overline{P} - \overline{P_n} \geq \alpha\left(\frac{1.28\overline{P_n}}{N^{\frac{1}{2}}}\right)$$

where $P_r(mW)$ is the power received by the radar antenna, P is the average total power, P_n is the average noise power, and the term $\alpha(1.28P_n \ x \ N^{-1/2})$ is the minimum detectable signal based on the standard deviation of average N noise and α, the parameter adjusted

to change the criterion for cloud detection (Clothiaux 1995). The criterion for significant detection is used to create a "cloud binary mask image" from the initial radar reflectivity data. Then, in order to derive a final mask of significant hydrometeor detection, a series of filters are applied to the criterion. Although drizzle and precipitation can lead to errors in cloud base determination, the 94-GHz radar using the described detection algorithm successfully detected cloud boundaries, especially in boundary layer clouds and cirrus clouds.

The ground-based micropulse lidar (MPL) is an effective tool for the detection of hydrometeors within a column (Clouthiaux et al. 1998). A cloud detection algorithm developed for use by the MPL at the U.S. Department of Energy's Atmospheric Radiation Measurement (ARM) Southern Great Plains (SGP) site attempted to identify all significant power returns in a vertical column of the atmosphere to determine hydrometeor distribution. This algorithm intended to accurately detect the cloud base height of optically thin clouds that frequently go undetected by the 94-GHz radar (Clothiaux et al. 1998). Power returned from clear days was used as the basis to calibrate the power returned when a cloud layer was present in the sampled column in order to optimize hydrometeor detection. The algorithm significantly improved previous methods of detecting high-level cirrus clouds.

In September 1994, NASA flew a three-wavelength backscatter lidar as part of the Lidar In-Space Technology Experiment (LITE) on board the Space Shuttle Discovery (Winker et al. 1996). LITE was the first lidar principally dedicated to atmospheric studies to fly in space. The primary objective of the LITE mission was to show that lidar technology serving as a space-based remote sensing tool could provide considerable knowledge about the vertical structure of clouds and aerosols in the atmosphere. LITE captured, for the first time, multi-layered clouds from space and detected optically thin high clouds generally blocked by low-level clouds detected by ground-based sensing systems. In fact, LITE demonstrated that despite the expected total attenuation by thick boundary layer clouds or deep convective clouds, the lidar profiles penetrated to an

altitude of 1 km or less in 70% of all cloud cases (Winker et al. 2003). This successful mission demonstrated the usefulness of lidar technology on space-based platforms and paved the way for future lidar-equipped satellite missions.

Numerous independent studies of radar and lidar remote sensing systems mention the potential advantage of combining the strengths of these two remote sensing methods to further improve hydrometeor detection and characterization (Baedi 2002; Clothiaux et al. 1995; Clothiaux et al. 2000; Lhermitte 1988). Cloud microphysical properties detected by one remote sensing method applied to another remote sensing data set can potentially resolve hydrometeor characteristics for an entire column. When spread over temporal and spatial domains, this information can provide comprehensive information about the current state of the atmosphere. The launch of the A-Train satellite constellation in 2006 presented the first opportunity for the synergistic collection of atmospheric data from a variety of space-based remote sensing systems. Specifically, the combination of the CloudSat 94-GHz radar and CALIPSO's CALIOP lidar provides accurate detection of hydrometeors through an entire atmospheric column.

C.   SCOPE OF RESEARCH

The objective of this research is to use combined CloudSat and CALIPSO data to remotely determine cloud base heights. Remotely determined cloud base heights are validated against ground-base lidar measurements from three of the U.S. Department of Energy's Atmospheric Radiation Measurement (ARM) Program. Chapter II describes these the CloudSat and CALIPSO remote-sensing systems in detail, including the detection algorithms used by each system. In Chapter III the data collection and evaluation process is outlined. This chapter includes descriptions of the ARM locations as well as the detection algorithms used by the ground-based instruments. Chapter IV covers the results and findings of the validation process. Chapter V presents suggestions for future research.

II. REMOTE SENSING SYSTEMS

A. A-TRAIN

The A-Train satellite constellation is a system of five satellites flying in formation. Formation flying provides a distinctive ability to collect information about a variety of Earth environment parameters in a synergistic manner (Goddard Space Flight Center 2003). These five satellites fly in close proximity to one another, allowing for nearly concurrent data collection from the different sensors. (Note: A sixth satellite, the Orbiting Carbon Observatory (OCO), was lost during launch in February 2009.) The A-Train is a sun-synchronous afternoon constellation, crossing the equator around 1330 local time each day. The constellation repeats its ground track roughly once every 16 days. While each remote sensing system in the constellation is individually valuable, the comprehensive atmospheric assessment provided by the constellation is unprecedented.
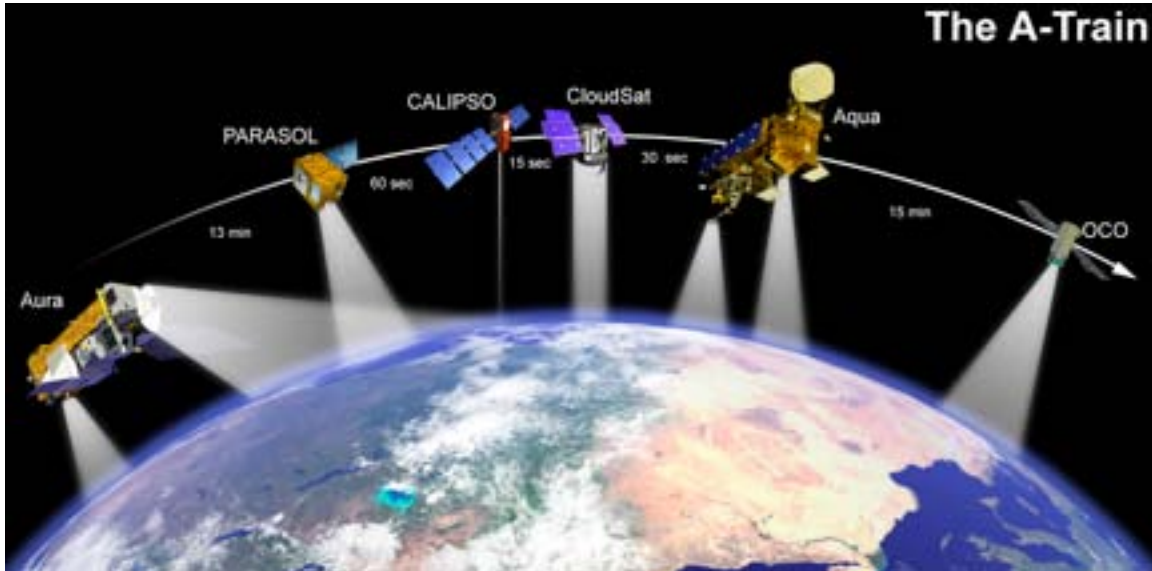
Figure 1.   Conceptual drawing of A-Train satellite constellation. The Orbiting Carbon Observatory (OCO) is schedule for launch in late February 2009. Image credit: NASA (http://www.nasa.gov/images/content/112931main_a-train.jpg).

Each of the satellites flying in the A-Train constellation carries sensors collecting specific data. The Aqua satellite leads the formation and carries six sensors on board: the Atmospheric Infrared Sounder (AIRS), the Advanced Microwave Sound Unit (AMSU), the Humidity Sounder for Brazil (HSB), the Advanced Microwave Scanning Radiometer-EOS (AMSR-E), the Clouds and Earth's Radiant Energy System (CERES), and the Moderate Resolution Imaging Spectroradiometer (MODIS). This sensor payload captures synergistic measurements of water in its various forms on Earth's surface and in the atmosphere along with global climate data (Goddard Space Flight Center 2003).

CloudSat follows Aqua in the A-Train constellation. This satellite carries a 94-GHz Cloud Profiling Radar (CPR). Following just behind CloudSat is the Cloud-Aerosol Lidar and Infrared Pathfinder Satellite Observations (CALIPSO). CALIPSO carries a payload of three instruments: the Cloud Aerosol Lidar with Orthogonal Polarization (CALIOP), a three-channel Imaging Infrared Radiometer (IIR), and a single-channel high resolution Wide-Field Camera (WFC) (Goddard Space Flight Center 2003). More information regarding these two satellite systems is presented in later sections of this chapter.

The next satellite in the A-Train formation is PARASOL, short for Polarization and Anisotropy of Reflectances for Atmospheric Sciences couple with Observations from a Lidar. PARASOL carries a sensor that measures polarization of light at eight different wavelengths in order to characterize hydrometeors and aerosols in the atmosphere (Goddard Space Flight Center 2003). The final satellite in the constellation is Aura. Aura's mission focuses on the monitoring of air quality, stratospheric ozone, and climate change (Goddard Space Flight Center 2003). This satellite carries a payload of four instruments: the High Resolution Dynamics Limb Sounder (HIRDLS), the Microwave Limb Sounder (MLS), the Tropospheric Emissions Spectrometer (TES), and the Ozone Monitoring Instrument (OMI). This combination of sensors measure distributions of greenhouse gases and pollutants and serve as a monitor of global climate change parameters (Goddard Space Flight Center 2003).

B.   CLOUDSAT

1.   94-GHz Cloud Profiling Radar

CloudSat flies in a sun-synchronous orbit at an altitude of 705 km. The satellite carries a near-nadir pointing 94-GHz Cloud Profiling Radar (CPR) designed to record range-resolved profiles of backscattered power. The satellite travels at an along track velocity of seven km/sec and generates a vertical profile of the atmosphere every 1.1 km along track, resulting in a horizontal resolution of 1.4 km across track and 2.5 km along track (Mace et al. 2007a). The CPR emits a pulse every 3.3 microseconds, creating a vertical resolution of 480 meters. Each profile created by the CPR is divided into 125 vertical range bins. Rather than scanning the atmosphere, the CPR generates a two-dimensional cross-section of the atmosphere along its trajectory (Marchand et al. 2008). The minimum detectable signal of the radar is approximately -31 dBz.

To maintain the synergistic data collection relationship between the various A-Train sensors, CloudSat is burdened with maintaining a precise flying relationship with the EOS PM (Aqua) satellite flying 120 seconds ahead and with CALIPSO flying just 15 seconds behind. Mission requirements dictate that the CPR footprint must always fall within the central few kilometers of the Aqua MODIS swath while the CPR and CALIPSO ground footprints must overlap at least 50% of the time (Stephens et al. 2002). This tightly monitored synchronization allows for the fusion of data streams between the remote sensing systems that is central to the research presented here.

The CPR technology exploits the fact that clouds are weak scatterers of microwave radiation. Cloud reflectivity increases at higher frequencies, but so does atmospheric attenuation due to water vapor. The 94-GHz frequency optimizes sensitivity to weak scattering while minimizing significant atmospheric attenuation.   In addition to water vapor attenuation, absorption by liquid water droplets and precipitation cause additional attenuation. While attenuation due to water vapor is automatically corrected in each profile, attenuation due to liquid water droplets and precipitation must be addressed in specific retrieval algorithms.

2.   Hydrometeor Detection Algorithm

The purpose of CloudSat's hydrometeor detection algorithm, called Geometrical Profile, or GEOPROF, is to use the data from the CPR to identify levels within the vertical column that contain a significant radar echo return due to the presence of hydrometeors.   The echo return for each vertical volume in the column flagged with a significant echo is then translated into an estimated radar reflectivity factor (Stephens et al. 2002). This process starts by building a significant echo mask (SEM) to identify resolution volumes deemed to have a return significantly different from background noise and thus likely contain a hydrometeor. Following the same detection algorithms as described by Clothiaux et al. (1995, 2000), the measurement of power returned must account for the potential for false alarms (i.e., range volumes that returned a signal indicating the presence of hydrometeor when none actually exists). Power-returned from the vertical column combined with a Gaussian-like distribution of background noise added to the power returned reduces the likelihood of false alarms within the column. The initial criteria for a significant return based on this relationship is

$$P_{r,jk} > P_{n,jk} + (3\sigma_n)$$

where P_r is the sum of power returned from a resolution volume, P_n is the Gaussian-like background system noise power, the subscripts j and k represent the along track dimension and the vertical dimension of the resolution volume, respectively, and σ_n is the standard deviation of $P_{n,jk}$. If this criterion is met, the algorithm then calculates the radar reflectivity in this range volume for the CPR cloud mask. If the criterion is not originally met, a probability function that considers the possibility of noise in the range volume and noise statistics of its neighbors known not to contain a significant echo is applied to ensure the cloud mask is applied properly (Mace 2007). The SEM output includes the radar reflectivity factor for 125 levels in each column calculated from the returned echo power (P_r).

The SEM is then compared to MODIS data from the EOS PM (Aqua) satellite flying just five seconds ahead of the CloudSat ground track. The comparison between the SEM and the MODIS cloud mask serves as a quality check of the GEOPROF output.

The MODIS cloud mask includes a detailed 48-bit cloud scene classification for every 1-km horizontal resolution pixel. Because the MODIS pixel is smaller than the 1.4-km across track by 2.5-km along track resolution of the CPR, a weighting scheme is applied to the MODIS pixels to ensure comparison to the correct CPR range volumes. The CPR then produces its own CPR Cloud Mask signaling whether or not a cloud is detected. The GEOPROF product also provides information about the variability of the scene via comparison of the fraction of MODIS pixels within the CloudSat footprint comprised of the same cloud type (Mace 2007). The comparison of the two data streams is an important quality check. If the correlation between MODIS and CloudSat cloud placement is high, then higher order algorithms, like 2B-GEOPROF-Lidar product that is the focus of this research, can be used with confidence.

C.   CALIPSO

1.   CALIOP

The Cloud-Aerosol Lidar with Orthogonal Polarization (CALIOP) is the primary instrument on board the CALIPSO satellite. The instrument measures total backscatter within an atmospheric profile at two wavelengths: 1064 nm and 532 nm. Two separate 532 nm channels measure the polarization of the backscattered signal; one measures the backscattered signal parallel to the outgoing beam while the other measures perpendicular to the outgoing beam. The collected backscattered returns provide vertical distributions of aerosols and clouds as well as information about cloud ice/water phase and classification of aerosol size (Winker 2006). The satellite carries two redundant Nd:YAG lasers that produce simultaneous pulses at 1064 nm and 532 nm at a pulse repetition frequency of 20.2 Hz, a pulse length of approximately 20 nsec, and each laser produces 110 mJ of energy. The sampling frequency of the backscattered signals is 10 MHz. The beam diameter at Earth's surface is 70 m (Winker et al. 2003).

The fundamental vertical and horizontal sampling resolutions of the lidar are 30 m and 333 m, respectively, yielding a profile of 1400 30-m samples between 40 km and -2 km altitude (Winker et al. 2004). Initially the 532 nm channels are averaged to a 30 m

vertical resolution while the 1064 nm channel is averaged to 60 m. The column is sampled at the full 30-m resolution in the lower levels of the troposphere where spatially variable clouds and aerosols require the highest resolution to optimize detection. This resolution is not necessary in the upper troposphere and stratosphere where hydrometeors are neither as numerous nor as spatially-variable; thus, an on-board averaging scheme reduces the vertical resolution in the upper troposphere and again in the stratosphere. Table 1 outlines the CALIOP resolutions throughout the column.

Table 1.   Spatial resolution of downlinked data from CALIPSO's CALIOP sensor (Winker et al. 2006).

Altitude Range (km)	Horizontal Resolution (m)	532 nm Vertical Resolution (m)	Profiles per 5-km	Samples per Profile
30.1 to 40.0	5000	300	1	33
20.2 to 30.1	1667	180	3	55
8.2 to 20.2	1000	60	5	200
-0.5 to 8.2	333	30	15	290
-2.0 to -0.5	333	300	15	5

2.   CALIOP Level 2 Algorithms

Most of the CALIOP Level 2 algorithms are based on the results of the LITE mission. The Level 2 algorithms use range-resolved profiles of attenuated backscatter coefficients for data processing (Vaughan et al. 2004). The objective of Level 2 processing for CALIPSO products is to determine layer heights and descriptive properties, perform layer identification and typing, and build profiles of cloud and aerosol backscatter and extinction coefficients. The Level 2 algorithms fall under three modules: the Selective Iterated BoundarY Locator (SIBYL) detects layers; the Scene Classification Algorithm (SCA) classifies these layers by type, and the Hybrid Extinction Retrieval Algorithms (HERA) performs extinction retrievals (Winker et al. 2006). For the purposes of this research, only the SIBYL and SCA algorithms are discussed here. The HERA algorithm is fully outlined in Part IV of the CALIOP Algorithm Theoretical Basis Document.

The SIBYL begins data processing by locating identifiable cloud and aerosol layers based on the strength of the backscatter signal. The algorithm then employs a multi-level averaging scheme. In a process called "feature clearing", thick clouds are identified in high resolution, single-shot profiles of 532 nm backscatter data and removed from the profile. The removed feature is replaced with a model of clear air and the data below the removed boundary is corrected for the removed attenuation, leaving a backscatter profile that would have been measured if the removed feature had not been present (Vaughan et al. 2002). The profile is scanned again at a coarser resolution using the same technique. The process iterates over three horizontal averaging resolutions: 5 km, 20 km, and 80 km. Figure 2 provides a visual reference of the process. The algorithm provides the vertical location of all features within the profile as well as the vertical extent of these features.
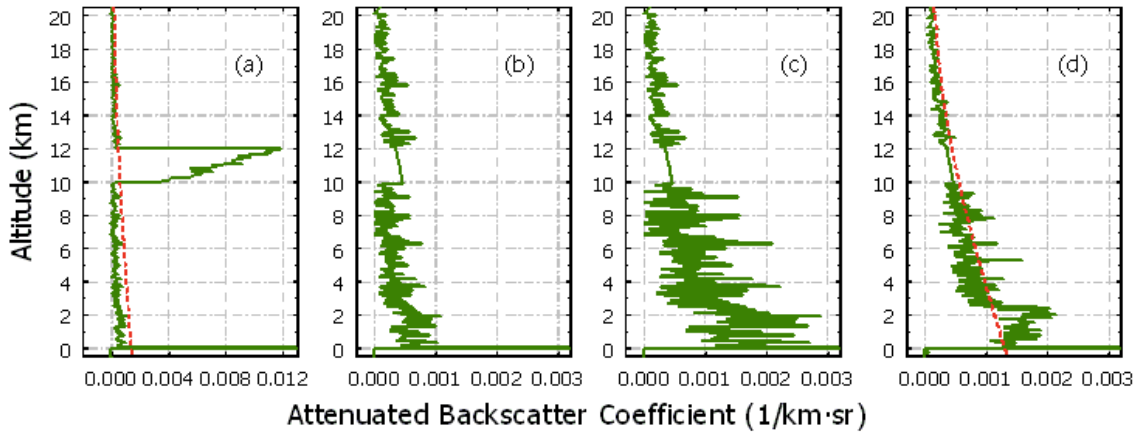
Figure 2. SIBYL Feature Clearing. Figure (a) shows a 5-km averaged profile with a moderate cirrus layer overlying a weaker absorbing aerosol layer. Figure (b) and (c) show, respectively, the removal of the cirrus layer and the correction of the underlying data for the estimated cirrus attenuation. Averaging four consecutive feature cleared 5-km profiles results in the 20-km horizontal average depicted in (d). This 20-km average reveals the previously obscured aerosol layer. The dotted lines in (a) and (d) are the threshold lines used by SIBYL's profile-scanning algorithm (Vaughan et al. 2002).

The SCA processes the features detected by the SIBYL and classifies the feature as either cloud or aerosol. The determination between cloud and aerosol is primarily based on scattering strength and spectral dependence on backscatter (Winker et al. 2006).

The cloud layers are then classified by cloud phase, either ice or water, based on the 532 nm depolarization signal profiles. A full description of the SCA is available from Liu et al. (2005). Each classification parameter is stored for the use in the Vertical Feature Mask (VFM).

3.   Vertical Feature Mask

The vertical feature mask (VFM) product provides the "where" and "what" information about the column. The VFM compiles outputs of the SIBYL and SCA to provide a spatial and morphological depiction of each lidar profile.   The mask is an array of bit-mapped integers, with each integer containing a set of scene classification flags for each range resolution element (Vaughan et al. 2004). The classification flags define the feature presence and feature type at that level. Table 2 details the bit interpretation for the VFM.

Table 2.   Bit interpretation for the CALIPSO Vertical Feature Mask (Vaughan et al. 2004).

Bit(s)	Field Description	Bit Interpretation	
1-3	Region type (there are $2^3 = 8$ possible classifications)	0 = invalid (bad or missing data) 1 = "clear air" 2 = cloud 3 = aerosol	4 = stratospheric feature 5 = surface 6 = subsurface 7 = no signal (totally attenuated)
4-5	Region type QA (there are $2^2 = 4$ choices)	0 = none 1 = low	2 = medium 3 = high
6-7	Ice/water phase (clouds only)	0 = unknown/not determined 1 = ice	2 = water 3 = mixed phase
8-9	Ice/water phase QA	0 = none 1 = low	2 = medium 3 = high
10-12	Cloud type (if region type = 2)	0 = not determined 1 = thin low overcast 2 = thick low overcast 3 = broken, low 4 = altocumulus	5 = transparent cirrus 6 = altostratus, nimbostratus, or cumulonimbus 7 = other
	Aerosol type (if region type = 3)	0 = not determined 1 = clean marine 2 = dust 3 = polluted continental	4 = clean continental 5 = polluted marine 6 = smoke 7 = other
	Stratospheric feature type (if region type = 4)	0 = not determined 1 = non-depolarizing PSC 2 = depolarizing PSC	3 = non-depolarizing aerosol 4 = depolarizing aerosol
13-14	Feature type QA	0 = none 1 = low	2 = medium 3 = high
15-17	Horizontal averaging required for detection	0 = not applicable 1 = 1/3-km 2 = 1-km	3 = 5-km 4 = 20-km 5 = 80-km
18-32	spare		

D.   COMBINED CLOUDSAT / CALIPSO PRODUCT

The 2B-GEOPROF-Lidar product combines the unique remote-sensing abilities of CloudSat's CPR and CALIPSO's CALIOP into a single product intended to provide a complete assessment of cloud and aerosol in the atmosphere. The combination of these two data sets allows for an estimate of cloud in each vertical radar bin and provides the heights of hydrometeor layer base and layer top for up to five different layers in each CPR vertical scan profile. The CPR is able to penetrate optically thick clouds, while the CALIOP can detect thin hydrometeor layers, such as thin high-level cirrus layers, below the CPR's detection threshold. The CALIOP also has a higher vertical and horizontal resolution than the CPR (see previous sections for horizontal and vertical resolutions of each instrument).

The algorithm used in creating the 2B-GEOPROF-Lidar product pulls the spacecraft latitude and longitude from the CPR Level 2B-GEOPROF product, along with the height of each radar bin and the radar significant echo mask. The algorithm then pulls the latitude and longitude of the lidar profile along with the vertical feature mask from the CALIPSO Level 2 Vertical Feature Mask product. The difference in horizontal resolution between the two instruments introduces the potential for pointing uncertainty, as shown in Figure 3.

To counter the uncertainty within the spatial domain, a weighting scheme is applied, in which the degree of contribution from a lidar observation to a specific radar observation is calculated in terms of the degree to which that particular lidar observation potentially contributed to the spatial overlap in the radar observational domain. This weighting scheme is defined as

$$w_i = \int\limits_x \int\limits_y P_r P_l^i \, dy \, dx$$

where i counts the lidar profile in a particular radar observational domain, x and y define the spatial dimensions to form an area enclosing the radar spatial domain, P_r and P_l are the spatial probability that a particular element in the area defined by x and y contributes to the observation of the radar and lidar, respectively. Using this weighting function, an

13

acceptable lidar cloud fraction at any level within the radar's footprint can be expressed as a weighted combination of the lidar observations within the radar field, as shown by the following equation:

$$C_l = \frac{\sum_{i=1}^{\# \, of \; lidar \; obs} w_i \delta_i}{\sum_{i=1}^{\# \, of \; lidar \; obs} w_i}$$

Here C_l is the lidar cloud fraction, i is the number of lidar observations within a particular radar resolution volume, and δ_i is the lidar hydrometeor occurrence which indicates whether or not a hydrometeor exists at a given height within a given profile (Mace et al. 2007b). Essentially, C_l quantifies partial filling of a specific radar volume by hydrometeors, and can therefore be used to correct errant radar reflectivity values due to partial beam filling.
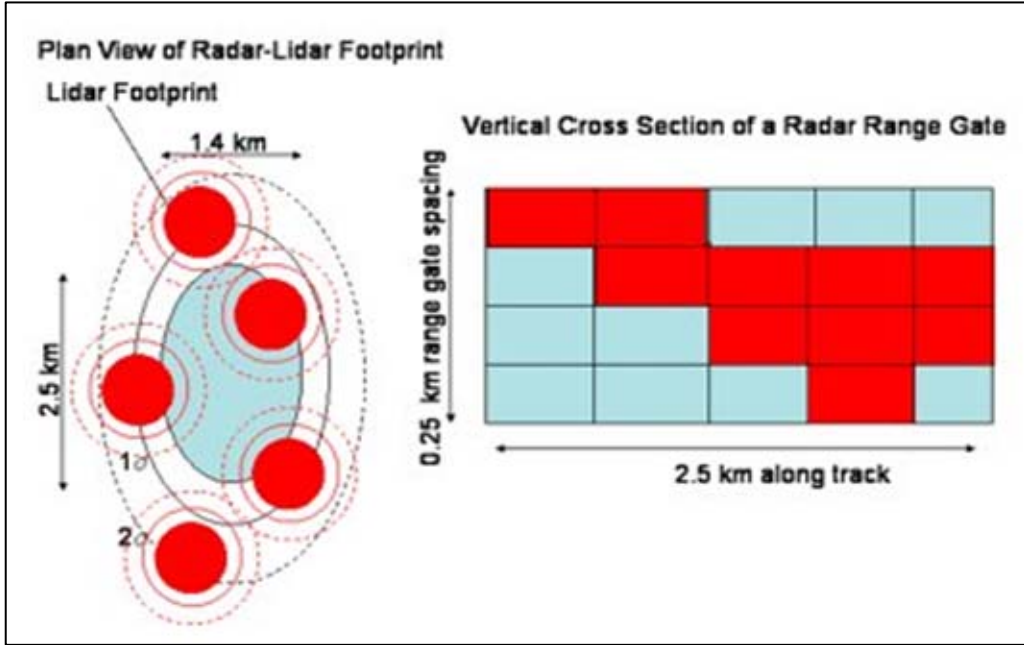
Figure 3.   Conceptual view of CPR-Lidar overlap. The diagram on the left is a plane view of a radar footprint in blue and lidar footprint in red. The black (red) solid and dashed ellipses (circles) represent the 1 and 2 standard deviation pointing uncertainty of the radar (lidar). The diagram on the right is a vertical cross section of a radar range resolution volume. The squares represent potential lidar resolution volumes that contain hydrometeors as reported by the lidar Vertical Feature Mask (VFM) product (Mace et al. 2007b).

14

The 2B-GEOPROF-Lidar produces a layer product that uses the combined cloud masks from both the radar and lidar to define the base and top height of up to five hydrometeor layers within a column. The product identifies whether the layer is detected by the radar or the lidar. Due to the finer vertical resolution of the lidar (30 m versus 480 m), the lidar serves as the default instrument when reporting a layer boundary height. If the lidar identifies the layer boundary top but the signal fully attenuates before reaching a layer boundary base, the boundary top indicator will show detection by the lidar while the boundary base indicator will show detection by the radar. If the observed layer boundary falls within the same range bin for both the lidar and radar, the boundary height is defined by the lidar due to its finer resolution, while the instrument contribution flag would indicate that both instruments observed the boundary.

The final output of the CPR 2B-GEOPROF-Lidar Product provides cloud volume fraction and uncertainty of this fraction, the number of hydrometeor layers detected in the vertical column (up to five layers), the height of the cloud layer top and cloud layer base, and the instrument flag indicating which remote sensing instrument observed the cloud base and top. For the purposes of this research, the height of the cloud layer base and the instrument flag are the primary fields of interest.

THIS PAGE INTENTIONALLY LEFT BLANK

III. DATA COLLECTION AND ANALYSIS

A. GROUND-TRUTH COMPARISON

The initial research compared cloud based height assessments from the combined CloudSat / CALIPSO 2B-GEOPROF-Lidar product to data from four ARM sites: the Southern Great Plains (SGP) site near Lamont, Oklahoma; the North Slope of Alaska (NSA) site near Barrow, Alaska; and the Tropical West Pacific (TWP) sites of Manus Island, Papua New Guinea and Darwin, Australia. The 2B-GEOPROF-Lidar product is compared to the Active Remote Sensing of Clouds (ARSCL) value-added product (VAP) cloud base height product (*arsclcbh1cloth,* here after referred to as "ARM Cloud Base Height") from each of these four sites. This product combines data from a co-located 35-GHz millimeter cloud radar (MMCR), a micropulse lidar, and Vaisala laser ceilometer (Clothiaux et al. 2000) to construct a best estimate of cloud-base height over the ARM site. The complete detection algorithm used in construction of the *arsclcbh1cloth* product is detailed in Clothiaux et al. (2000).

Due to the small ground footprint limiting spatial and temporal coverage of CloudSat and CALIPSO, all 2B-GEOPROF-Lidar data within a 20-km radius of each ARM location was pulled for the comparison. For the Manus Island site the radius was expanded to a 50-km radius of the ARM ground site in order to capture an adequate number of satellite overpasses for the dataset. The cloud base height reported by the ARM Cloud Base Height data was accepted as ground truth for the comparison. The difference in reported cloud base altitude between the 2B-GEOPROF-Lidar product and ARM Cloud Base Height product was calculated for a temporal window of two minutes on either side of the closest satellite nadir overpass to the ARM ground site, along with the distance from the nadir overpass point to the ground site. Figure 4 is a graphical representation of this data comparison. The two-minute buffer on either side of the nearest nadir overpass time was chosen for trend analysis purposes only. With the satellite constellation traveling at a relative ground speed of seven km/s, the satellite observations at the temporal extremes of the two-minute window are roughly 840 km

away from the ARM ground site, and therefore no correlation to the ARM Cloud Base Height assessment was expected at the extremes. Altitude differences greater than 720 m (1.5 times the vertical resolution of CloudSat) were labeled as significant outliers for further investigation.
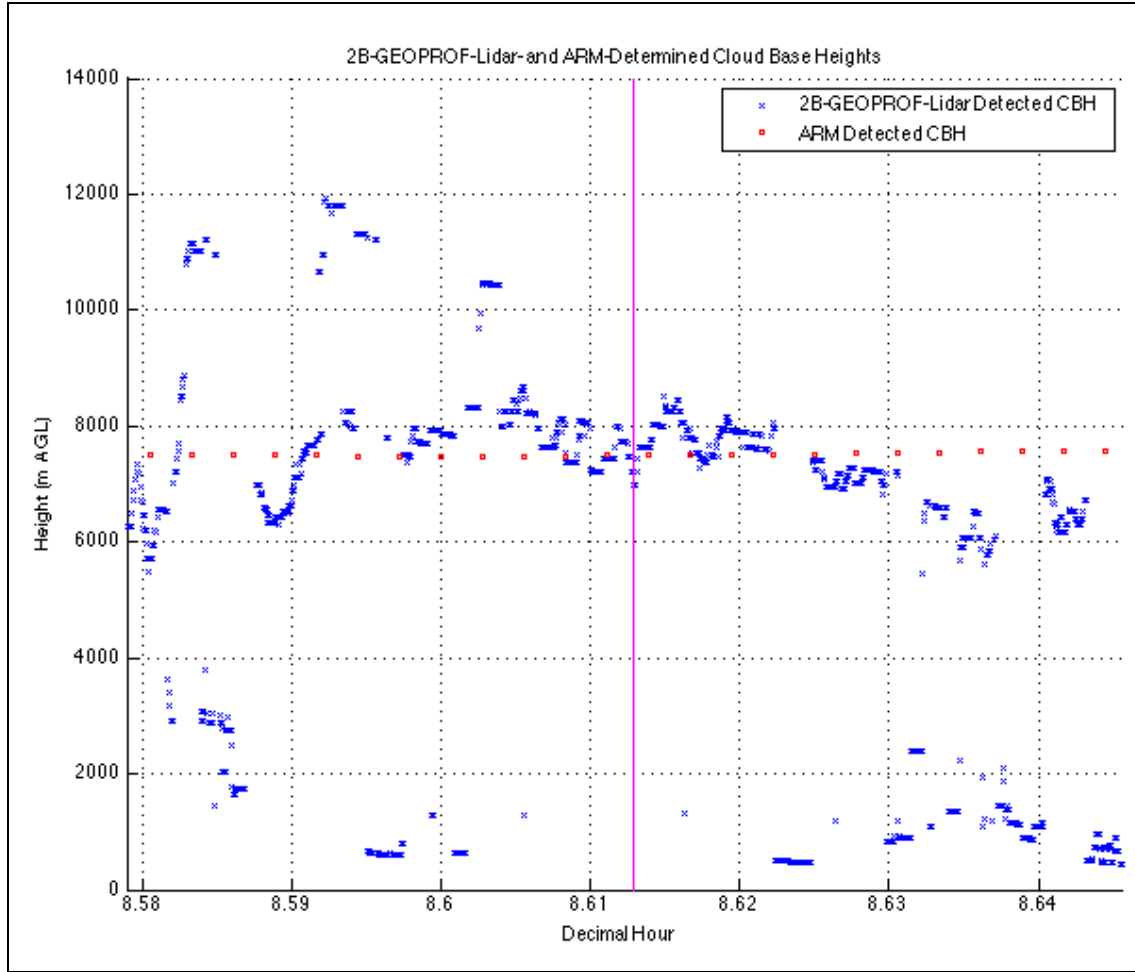
Figure 4.   Plot of 2B-GEOPROF-Lidar cloud base heights (blue 'x') and ARM Ground Site cloud base heights (red squares) for SGP site on 10 October 2006. Magenta line denotes nadir of closest satellite overpass to ground site, with +/- 2 minutes of data plotted on either side of overpass.

The first step in investigation of the outliers was a visual inspection of Aqua MODIS imagery. The likelihood of a direct satellite overpass of the ARM ground site is low given the small footprint of both CloudSat and CALIPSO. The MODIS imagery was used to ensure that the cloud element detected by ground site was similar to the cloud

feature detected by CloudSat and CALIPSO. Local METAR observations were also compared to the cloud base data as a supplemental accuracy check. These local observation points and distances from the nearest ARM ground site are listed in Table 3. Any outliers of cloud base heights within 720 m of the locally observed cloud base were marked as acceptable measurements and removed from the significant outlier pool.

Table 3. Supplemental observation points and distance from respective ARM ground site.

ARM Site	Local Observation Point	ICAO	Distance from ARM Site
SGP	Enid Woodring Regional Airport	KWDG	37.42 km
	Ponca City Regional Airport	KPNC	46.36 km
NSA	Barrow Airport	PABR	6.82 km
TWP-Darwin	Darwin International Airport	YPDN	1.93 km
TWP-Manus	Momote Airport	AYMO	6.23 km

After narrowing the outlier pool based on the MODIS and local observations, the instrument responsible for the measurement—either CloudSat or CALIPSO—was noted. The outliers were then further investigated with additional products from each satellite system, with special interest placed on those products from the responsible remote sensing system, as outlined in the following sections.

B. ADDITIONAL CLOUDSAT ANALYSIS

The CloudSat 2B-GEOPROF product provides radar reflectivity (Z_e) and a cloud mask for each sampled column. The Z_e data is calculated from the echo power measurements recorded by CloudSat's Level 1B science data. Z_e values range from -40 to 50 dBZ. The cloud mask is created from the SEM outlined in Chapter II. The mask assigns a cloud probability to each significant echo return within the column, with values

between 20 and 40 indicating the detection of a cloud. Increasing values represent clouds with a lower chance of being a false detection (Marchand et al. 2007).

Figures 5 and 6 show an example of radar reflectivity and the cloud mask plots, respectively, for a five-minute window on either side of the closest satellite overpass of the ARM site. The 2B-GEOPROF product provides both Z_e and the cloud mask for each of the 125 layer bins in the vertical column sampled by CloudSat. The values of Z_e and the cloud mask corresponding to the layer containing the cloud base were compared, noting any discrepancies or trends. The results of this analysis are reported in Chapter IV.
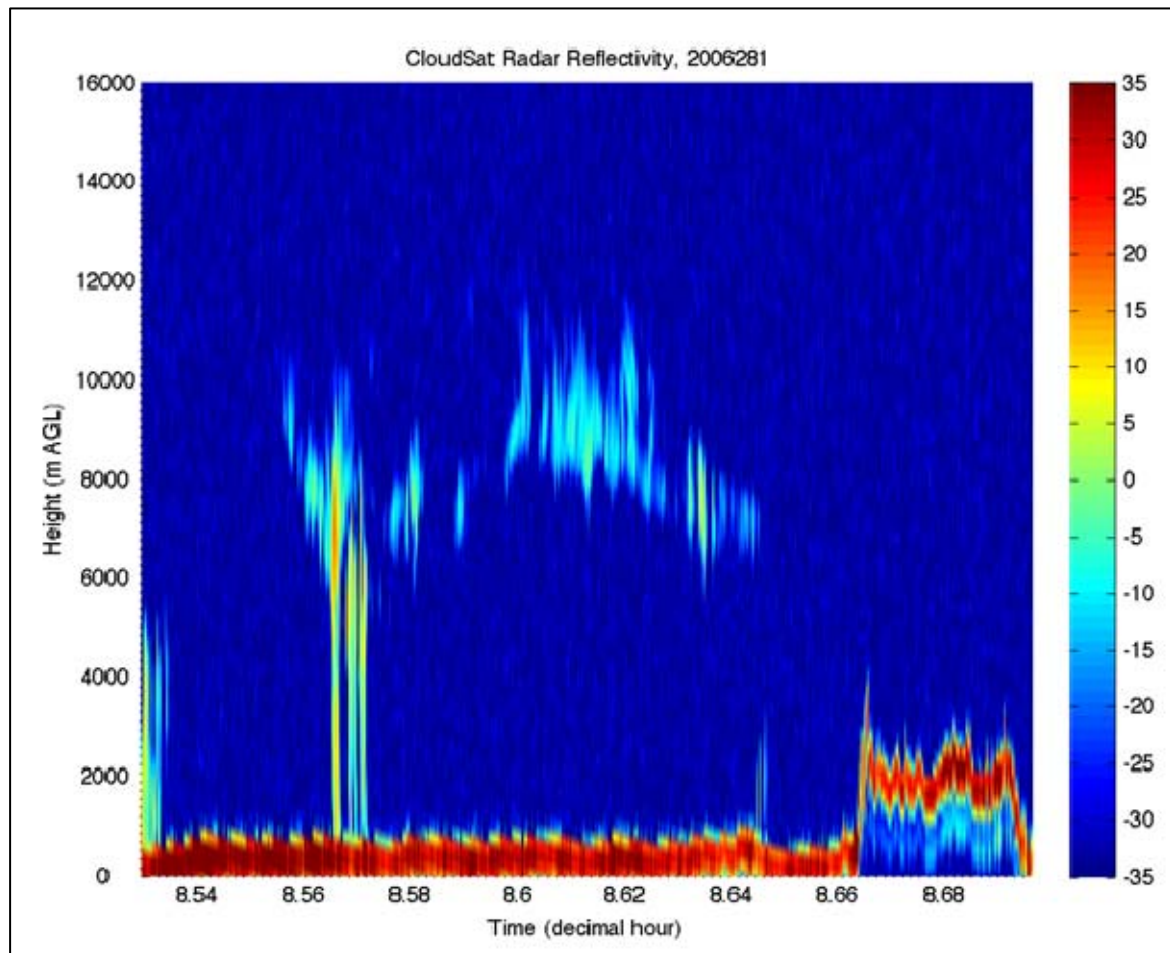
Figure 5.   Plot of Radar Reflectivity from CloudSat CPR 2B-GEOPROF data, 8 October 2006 (Julian Date: 281). CloudSat's nearest overpass to the SGP ARM site occurred at 0836 UTC (decimal hour: 8.6122). Color bar represents dBZ values. Data plotted +/- 5 minutes of overpass.
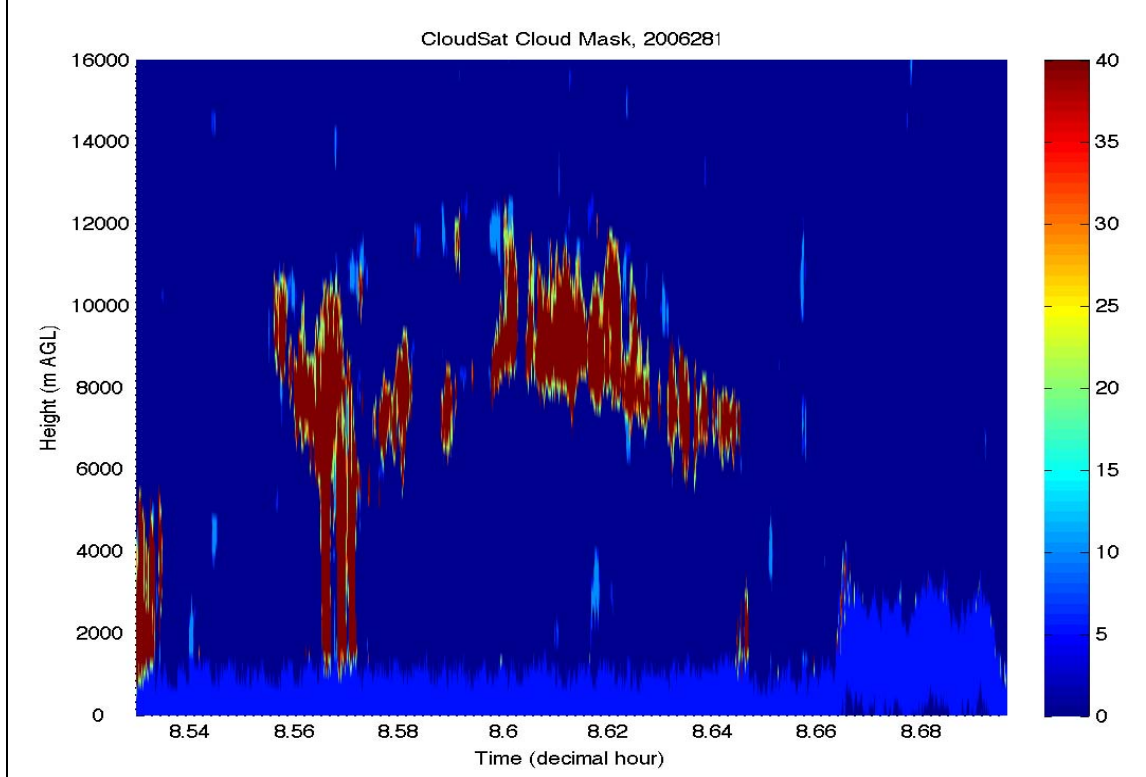
Figure 6.   Plot of the cloud mask from CloudSat CPR 2B-GEOPROF data, 8 October 2006 (Julian Date: 281). CloudSat's nearest overpass to the SGP ARM site occurred at 0836 UTC (decimal hour: 8.6122). Increasing Cloud Mask values indicate increasing probability of cloud layer. Data plotted +/- 5 minutes of overpass.

In addition to providing Z_e and cloud mask information, the 2B-GEOPROF algorithm performs an inter-comparison of MODIS data and the SEM. The inter-comparison includes four fields used for further investigation of the outliers. First, a MODIS cloud flag is set that defines the confidence of cloud cover within the column (cloudy, uncertain clear, probably clear, and confident clear). The second field is a MODIS pixel cloudiness characterization based on the MODIS cloud mask (clear, high cloud, very thin high cloud, thin high cloud, thick high cloud, non-high cloud, thick mid cloud, and low cloud). The third field of interest is a classification of CPR cloud echo tops based on MODIS cloud characterization within the CPR footprint (clear profile, high cloud, mid level cloud, low level cloud, and multilayer clouds). Finally, the fourth field of interest is a CloudSat scene variability parameter that describes the fraction of MODIS

21

pixels in the vicinity of the CloudSat footprint with the same cloud type (high uniform, uniform, weakly variable, variable, and highly variable) (Marchand et al. 2007). These fields were investigated for each outlier, specifically noting trends within certain cloud classifications that challenged accurate cloud base height identification. Again, these results are presented in Chapter IV.

The final CloudSat product used in the investigation of the outliers was the Cloud Scenario Classification (2B-CLDCLASS) product. This product classifies clouds using vertical and horizontal cloud properties derived from 2B-GEOPROF Z_e and cloud mask data, the presence or absence of precipitation, and upward radiance measurements from MODIS (Wang and Sassen 2007), along with temperature data from ECMWF. The algorithm classifies clouds as cirrus, altostratus, altocumulus, stratus, stratocumulus, cumulus, deep cumulonimbus, or nimbostratus. The outliers were compared to the cloud type identified by the 2B-CLDCLASS product. This comparison served two purposes: (1) the comparison served as a quality check of the CloudSat data collection algorithms since the cloud base height and cloud type should show a degree of correlation, and (2) any repetitive trends in uncorrelated cloud base heights and cloud type potentially highlight biases and weaknesses in the cloud base height detection algorithm.

C.   ADDITIONAL CALIPSO ANALYSIS

CALIPSO Lidar Level 1B profile data provides total attenuated backscatter at 532 nm. The backscatter is reported at 583 levels in the vertical column. This fine vertical resolution was exploited in order to attempt to identify trends within the outlier pool. Furthermore, plots of the total attenuated backscatter data provided an additional visual reference for comparison with the CloudSat Z_e and cloud mask data plots.

In addition to the cloud base and cloud top height assessments for the column used in the 2B-GEOPROF-lidar product, the CALIPSO Level 2 Cloud and Aerosol Layer product also provides the integrated attenuated backscatter at 532 nm. For each hydrometeor layer detected, the product calculates the backscatter between the determined cloud base and cloud top for the layer. This backscatter data was compared across the outliers with trends noted.
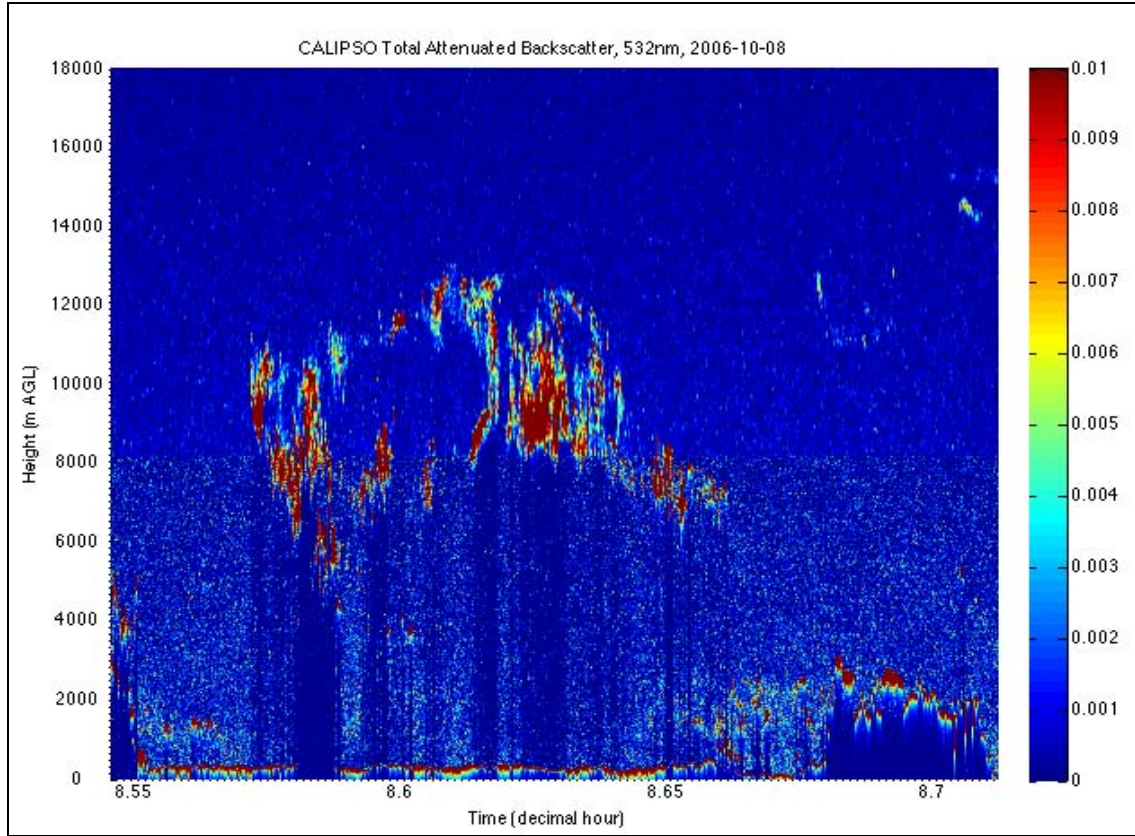
Figure 7.   Plot of total attenuated backscatter at 532 nm detected by CALIPSO on 8
           October 2006. CALIPSO's nearest overpass to the SGP ARM site occurred at
   0837 UTC (decimal hour: 8.6287). Data plotted +/- 5 minutes of overpass.

CALIPSO's Level 2 Cloud and Aerosol Layer product also provides a set of feature classification flags created by the Vertical Feature Mask (VFM) outlined in Chapter II. The product provides feature type (cloud, aerosol, or stratospheric layer), feature subtype (cloud type for the purposes of this research), and ice/water phase of the cloud. As was done with the CloudSat Cloud Scenario Classification data, the outliers were compared to the feature classification flags to find any correlation and/or trends in the falsely detected cloud base heights. Furthermore, since the primary product used for the initial cloud base height determination combines data from CloudSat and CALIPSO, the feature products from the two satellites were compared against each other for the outliers as a further check of accuracy. These results are reported in Chapter IV.

THIS PAGE INTENTIONALLY LEFT BLANK

IV. RESULTS AND FINDINGS

A. OVERALL RESULTS

The 2B-GEOPROF-Lidar product accurately identified the cloud base height in 73.22% of the cases examined. For the purposes of this research, an accurately identified cloud base height was defined as a cloud base reported by the 2B-GEOPROF-Lidar product that fell within 480 m of the ground-reported cloud base height. Table 4 summarizes the results for all four locations. Figure 8 provides a direct comparison of the 2B-GEOPROF-Lidar cloud base heights versus the ground site-detected cloud base heights. This figure highlights a few trends in the data. Any differences in cloud base height that exceeded 720 m (1.5 times the resolution of the CPR) were labeled as significant outliers and selected for further investigation. The four ARM locations represent drastically different climatic and geographic areas and the results reflect noticeably different trends for each location. While the independent results for each location are discussed in the later sections of this chapter, a few overarching trends are apparent in the combined analysis of all data points.

Table 4.   Results of comparison of cloud base heights between the CloudSat / CALIPSO 2B-GEOPROF-Lidar product and ground observations.

Location	Number of Samples	Number of Correct Detections	Percentage of Success	Distance from Nadir Overpass to ARM Ground Site (km)
SGP	35	26	.74	17.82
NSA	54	37	.69	20.37
TWP-Darwin	64	53	.83	7.46
TWP-Manus	30	18	.60	49.24
All Sites	183	134	.73	23.72
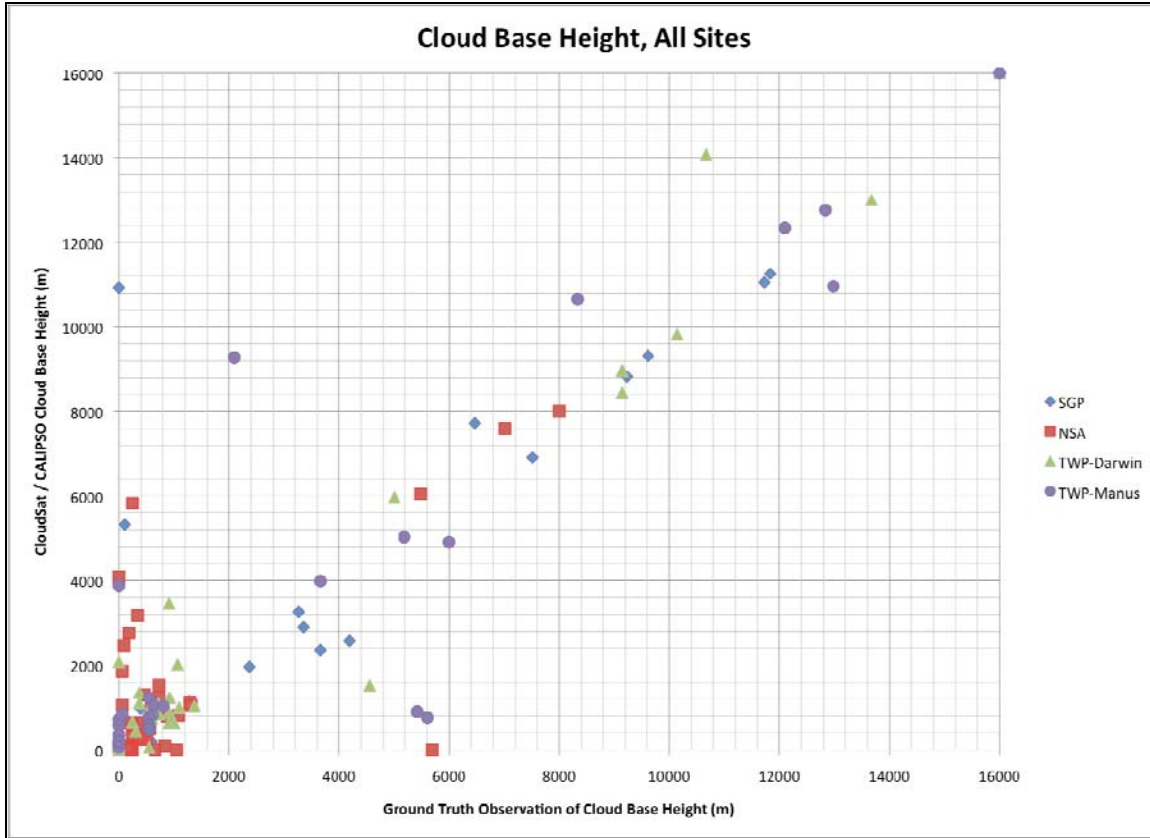
Figure 8.   Plot of CloudSat / CALIPSO-determined cloud base heights via the 2B-GEOPROF-Lidar product versus ground-based cloud base heights.

Since the 2B-GEOPROF-Lidar product indicates whether the reported cloud base height was determined by CloudSat or CALIPSO, this provided a focal point for the preliminary investigation of the outliers. For the complete data set, CALIPSO detected the cloud base in 82 of the 122 cases (67.21%) where a cloud was present in the column. Due to the higher resolution of the CALIOP and the nature of the 2B-GEOPROF-Lidar algorithm for cloud base height discussed in Chapter II, a greater number of CALIPSO detections was expected. CALIPSO correctly identified the cloud base height in 55 of the 82 cases (67.07%) where it was the primary detection instrument. Meanwhile CloudSat accurately identified the cloud base height in 19 of the 40 cases (47.50%) in which it was the primary detection instrument. The lower percentage of successful cases from CloudSat is attributed to the documented challenge of the CPR to resolve hydrometeors in the lowest kilometer of the atmosphere, which is further discussed later

26

in this section. There were six cases in which both CloudSat and CALIPSO failed to identify any significant hydrometeor layers in the column while the ARM instruments reported a layer. Figure 9 shows the distribution of CloudSat and CALIPSO plots for the data set.
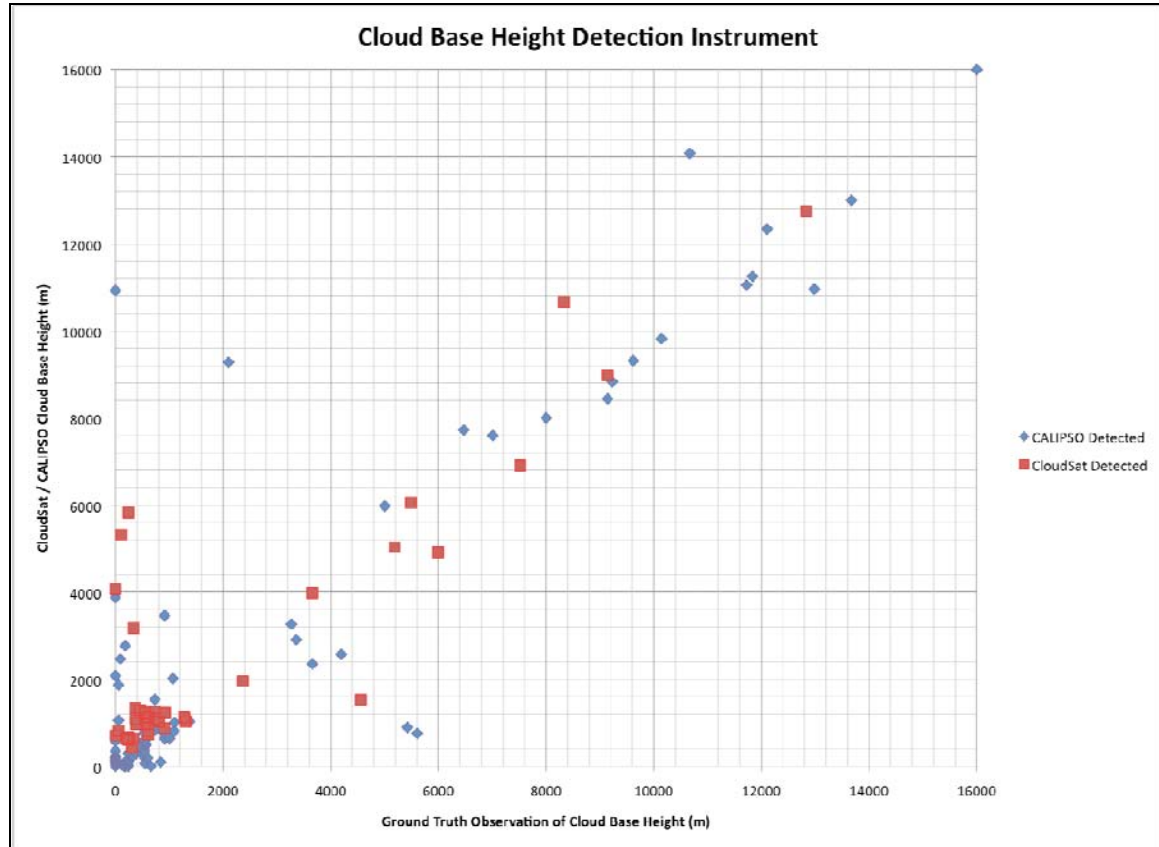
Figure 9.   Comparison of satellite-derived cloud base heights versus ground observation of cloud base height, sorted by primary detection instrument used by 2B-GEOPROF-Lidar product. ARM measurements from all fours sites are included in this figure.

A documented problem with the current 2B-GEOPROF-Lidar algorithm is CloudSat CPR's decreased sensitivity to hydrometeor detection in the lowest 1 km of the atmosphere due to a combination of surface reflection and the 1 km pulse length of the CPR (Mace et al. 2007b). According to the 2B-GEOPROF-Lidar documentation, no identifiable hydrometeor signal is detected in the lowest 500 m of each profile, while hydrometeors between 500 m and 1 km are detected at a reduced sensitivity (Mace et al. 2007b). The results in this research confirm this known data issue. The ground

measurements reported cloud bases below 500 m in 48 cases. The satellite-derived cloud base heights proved accurate in 62.5% of these cases. In seven of the 18 cases where the difference exceeded 480 m, CALIPSO detected a mid-level deck between roughly 2000 and 4000 m. In cases with a ground-reported cloud base below 500 m CloudSat was not the primary detection instrument unless CALIPSO was completely attenuated by a mid- or upper-level cloud deck. In these cases, CALIPSO did not record any attenuated backscatter values in the column below the level of complete attenuation. The 2B-GEOPROF-Lidar product then relied solely on radar reflectivity returns from CloudSat to determine the cloud base. This introduced another bias with the detection scheme. CloudSat generally showed increased radar reflectivity returns near the surface in the range of -22 to -28 dBZ when the ground sites reported cloud bases below roughly 800 m. These increased dBZ values were reported at levels well correlated to the ground-reported cloud base height. However, the cloud mask attributed the increased reflectivity values to ground clutter and did not label the returns as cloud. Fine-tuning the SEM algorithm could reduce the ground clutter bias for the low-level layers, but is beyond the scope of this research.

The 2B-GEOPROF-Lidar product identified several high-level cloud base heights that the ground sites failed to identify. While the highest concentration of these errant high clouds was observed at the Darwin site, all locations showed several cloud base heights indicative of high clouds while the ground sites reported either a clear sky or an error in hydrometeor detection. Occasionally, the further check of the outliers against local METAR observations resolved a few of these discrepancies in cloud base height since a human observer is able to detect a high-level cirrus deck at a height beyond the vertical detection limits of the ground-based instruments. However, as will be shown in the independent discussions of the data from both Darwin and Manus later in this chapter, the comparison to METAR observations introduces its own set of biases and limitations, and therefore, cannot resolve all high-cloud outliers.

B.   SOUTHERN GREAT PLAINS (SGP) RESULTS

The data availability window for the SGP site was July 4, 2006 to February 16, 2008.   All CloudSat and CALIPSO overpasses of the SGP ground site occurred at approximately 0836 UTC (0236 LST); thus, all overpasses occurred during darkness. The comparison of cloud base heights between the satellite sensors and the ground observations for the SGP site showed the best correlation of the four ground sites, with an accurate assessment of cloud base height reported by the 2B-GEOPROF-Lidar product in 74% of the cases examined. Figure 10 shows the results of the comparison for the SGP site. Five cases were deemed significant outliers and selected for further investigation.
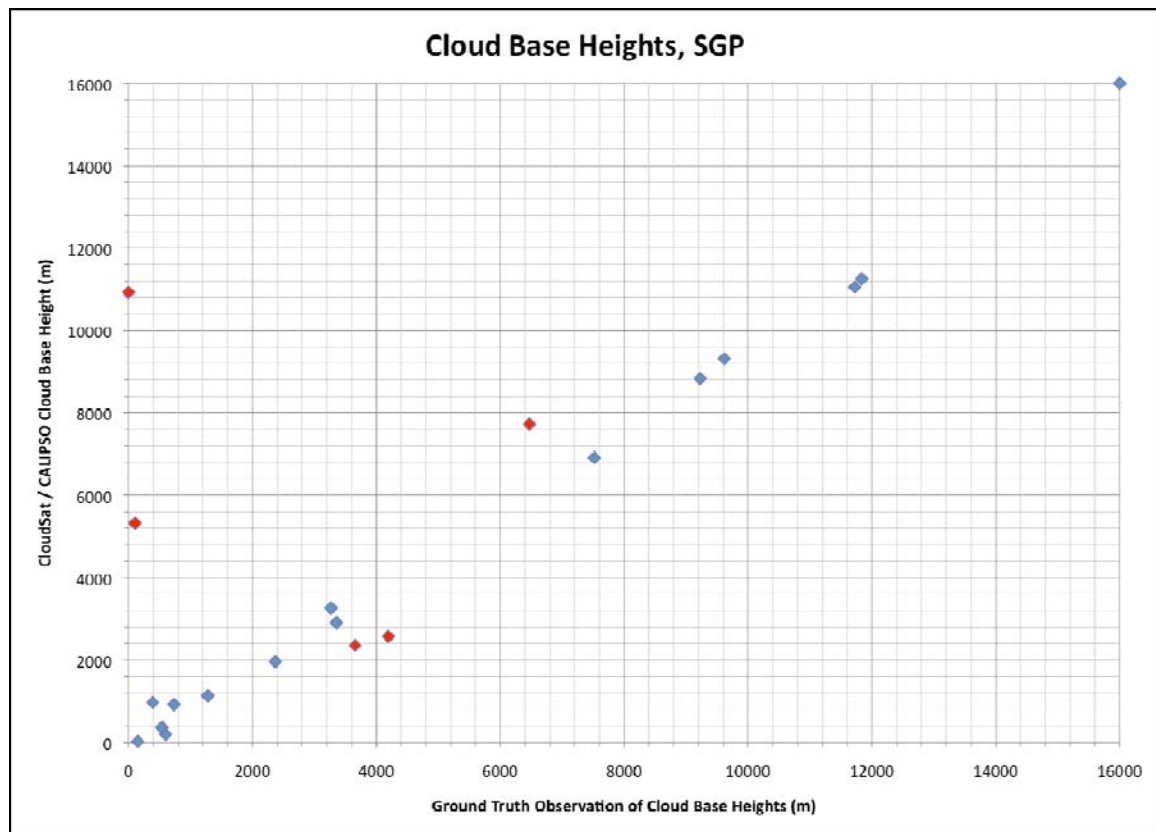

Figure 10.   Comparison of CloudSat / CALIPSO 2B-GEOPROF-Lidar cloud base heights versus ground-based assessment of cloud base height for the ARM SGP ground site. Red markers denote significant outliers (> 720 m difference).

Of the five outliers investigated, two cases occurred when the ARM ground site instruments reported the cloud base height at the surface and local METAR observations reported a broken or overcast deck at 30 m. MODIS imagery indicated the ground site was in the warm sector of a developing low-pressure system to the west in both cases. CloudSat returned slightly increased radar reflectivity returns (-19.58 dBZ and -22.73 dBZ) below 1000 m, but classified these returns as clutter and did not assign a cloud classification. CALIPSO also indicated the presence of hydrometeors in the lowest kilometer of the column with weak backscatter returns. In both cases CloudSat and CALIPSO do identify overlying mid- and upper-level cloud decks with strong correlation between respective radar reflectivity and layer backscatter returns. Figure 11 shows a MODIS image for one of the cases in question. Given the synoptic situation indicated in this satellite image, these elevated cloud layers certainly exist, but without a ground base measurement for confirmation, the verification of these cloud base height assessments is not possible.
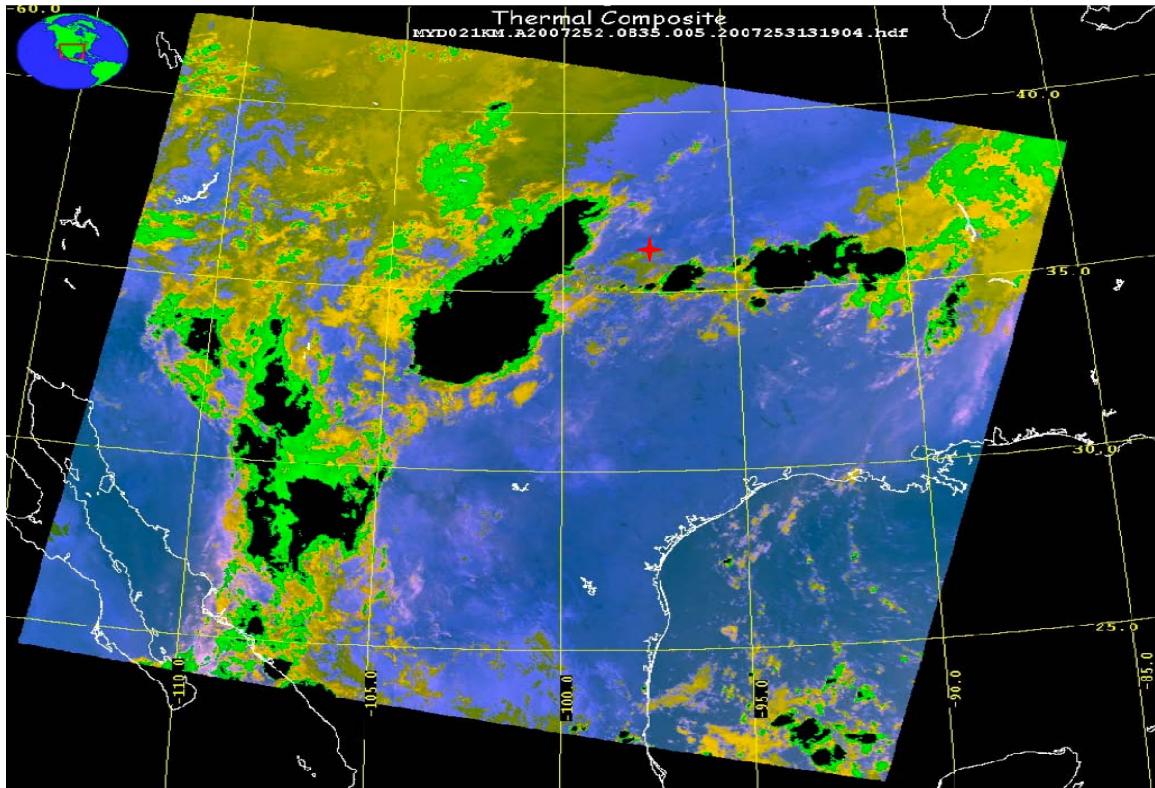

Figure 11. MODIS thermal composite image from 9 Sep 2007, 0835 UTC. Red cross represents location of SGP ARM ground site.

The three remaining outlier cases for the SGP ground site are cirrus situations. In one of these cases, both the CALIPSO Vertical Feature Mask (VFM) and the CloudSat cloud mask fail to identify a cloud in the column, and the local METAR reported clear skies. Furthermore, the CPR returned only weak radar reflectivity values of -29.6 dBZ at the levels labeled as cloud base by both the 2B-GEOPROF-Lidar and the ARM instrument. CALIPSO returned layer backscatter values indicative of a 240 m thick cirrus cloud. In this case, the more sensitive CALIPSO lidar detected a tenuously thin cloud that was not detectable by either the CloudSat CPR from above or the ground hydrometeor detection instruments. In the other two cirrus cases, CALIPSO was identified as the primary detection instrument of the cloud base height by the 2B-GEOPROF-Lidar data, and in both cases the assigned cloud base height was below the cloud base height detected by the ARM ground site. In these cases, both CPR radar reflectivity and CALIPSO total backscatter showed increased returns at the level indicated as the cloud base height by the ARM instruments, and the 2B-GEOPROF-Lidar product did assign a secondary cloud base at this indicated level in one of the cases. However, for the lowest cloud base identified by the 2B-GEOPROF-Lidar product, no significant increase in radar reflectivity or total backscatter occurred. The satellite-derived cloud base height assessment for the lowest cloud layer in both of these cases remained unresolved

C. NORTH SLOPE ALASKA (NSA) RESULTS

The data availability window for the NSA site was June 24, 2006 to December 26, 2007. The CloudSat and CALIPSO satellite overpass of the NSA ground site occurred at 1346 UTC (0446 LST) for the satellites' descending path or 2230 UTC (1330 LST) for the satellites' ascending path. Figure 12 shows the results of the comparison between the satellite-derived cloud base heights versus the ground-based observations.
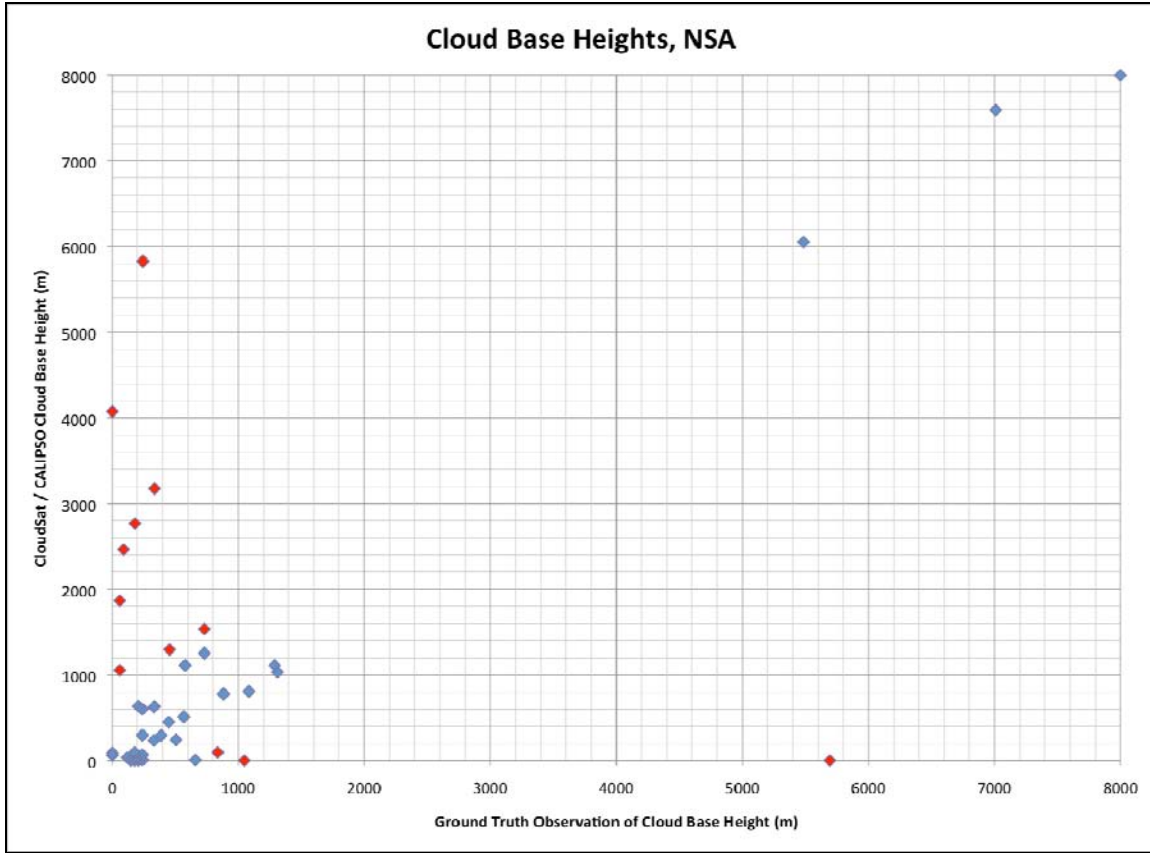
Figure 12. Comparison of CloudSat / CALIPSO 2B-GEOPROF-Lidar cloud base heights versus ground-based assessment of cloud base height for the ARM NSA ground site. Red markers denote significant outliers (> 720 m difference).

The most noticeable trend in Figure 12 is the satellite-derived cloud base heights reported much higher than the observed cloud bas heights in the lowest 500 m of the column. In fact, of the 12 significant outliers in the NSA data set, eight events occurred when the ground site reported a cloud base height below 1000 m and six of the events reported cloud base heights below 300 m. CloudSat showed increased radar reflectivity returns below 300 m for these six events, indicating the presence of hydrometeors. However, the cloud mask classified the increased returns as ground clutter rather than cloud. The cloud mask placed the cloud base at a higher level of increased reflectivity. Local METAR observations in three of these cases reported visibilities reduced to less than 1 km due to fog, and snow was reported in a fourth case, which is further discussed below. While the inability to accurately resolve the low-level cloud heights for the NSA

site was troublesome, this inaccuracy was expected due to the documented difficulties of the detection algorithms in the lowest 1 km of the sampled column.

One of the significant outliers was a snow event at NSA on 29 March 2007. The closest CloudSat overpass to the ARM ground site occurred at 1348 UTC. This was the only case where the satellite-derived cloud base height reported was lower than the ground observation when the ground sties reported a base below 1000 m. The CloudSat cloud classification reported a nimbostratus cloud with precipitation between 1280 m and 5597 m. Radar reflectivity values for this cloud feature ranged from -1.99 dBZ to -24.82 dBZ. The radar reflectivity returns remain high (> -17 dBZ) to 800 m, which also happens to be close to the 839 m cloud base detected by the ARM instruments, yet the cloud mask labeled the returns below 1280 m as ground clutter rather than cloud. The CALIPSO total attenuated backscatter data also indicated a cloud from 1630 m to 5530 m. The VFM reported a cloud base at 1587 m. Complete attenuation of the lidar occurred at approximately 1150 m, and no significant backscatter returns were received below this level. It is unclear why the 2B-GEOPROF-Lidar product detected a cloud base at 100 m, since neither the CPR nor CALIOP returned useful data from this level.

D. TROPICAL WEST PACIFIC - DARWIN RESULTS

The data availability window for the TWP-Darwin site was June 20, 2006 to April 23, 2008. The CloudSat and CALIPSO satellite overpass of the TWP-Darwin ground site occurred at 0506 UTC (1436 LST) for the satellites' ascending path or 1653 UTC (0223 LST) for the satellites' descending path. Figure 13 shows the results of the initial cloud base height comparison between the 2B-GEOPROF-Lidar and the ARM ground based detection.
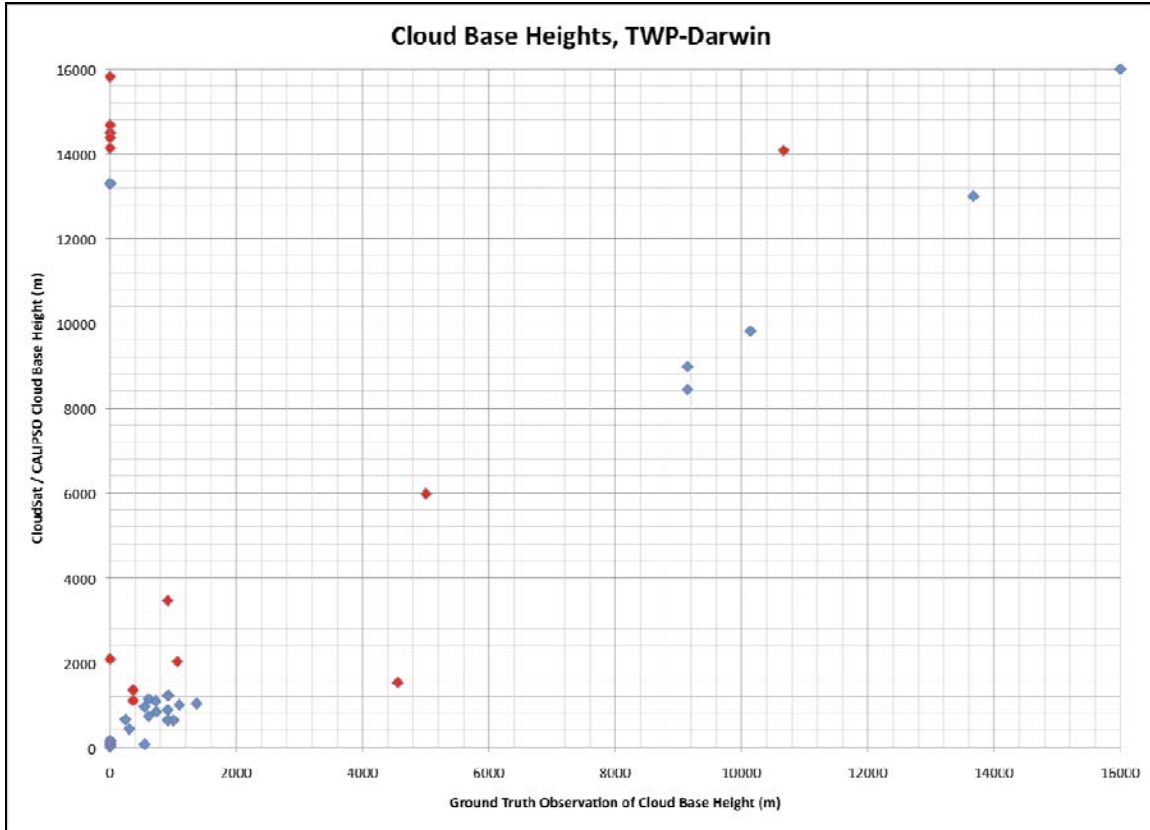
Figure 13.   Initial comparison of CloudSat / CALIPSO 2B-GEOPROF-Lidar cloud base heights versus ground-based assessment of cloud base height for the ARM TWP-Darwin ground site. Red markers denote significant outliers (> 720 m difference).

The initial results showed a sizeable group of significant outliers in which the satellite-assigned cloud base heights are much higher than the height assigned by the ARM instruments. The cloud base height reported by the ARM instruments in these cases was either 0 or reported as an error, while the satellite-derived cloud base heights exceeded 12500 m. Usually the METAR was referred to as the default cloud base height for validation purposes when the ARM site did not report a valid cloud base. However, the METAR observations from the Darwin International Airport used for validation simply reported "CAVOK" in each of these cases, indicating that no cloud was present below 1524 m, but providing no information about the atmosphere above this level. After a visual inspection of MODIS satellite imagery to confirm generally clear skies,

eight of these outliers were reclassified as clear profiles and removed from the outlier pool. Figure 14 shows the updated comparison of cloud base heights after correcting for the high-level clouds.
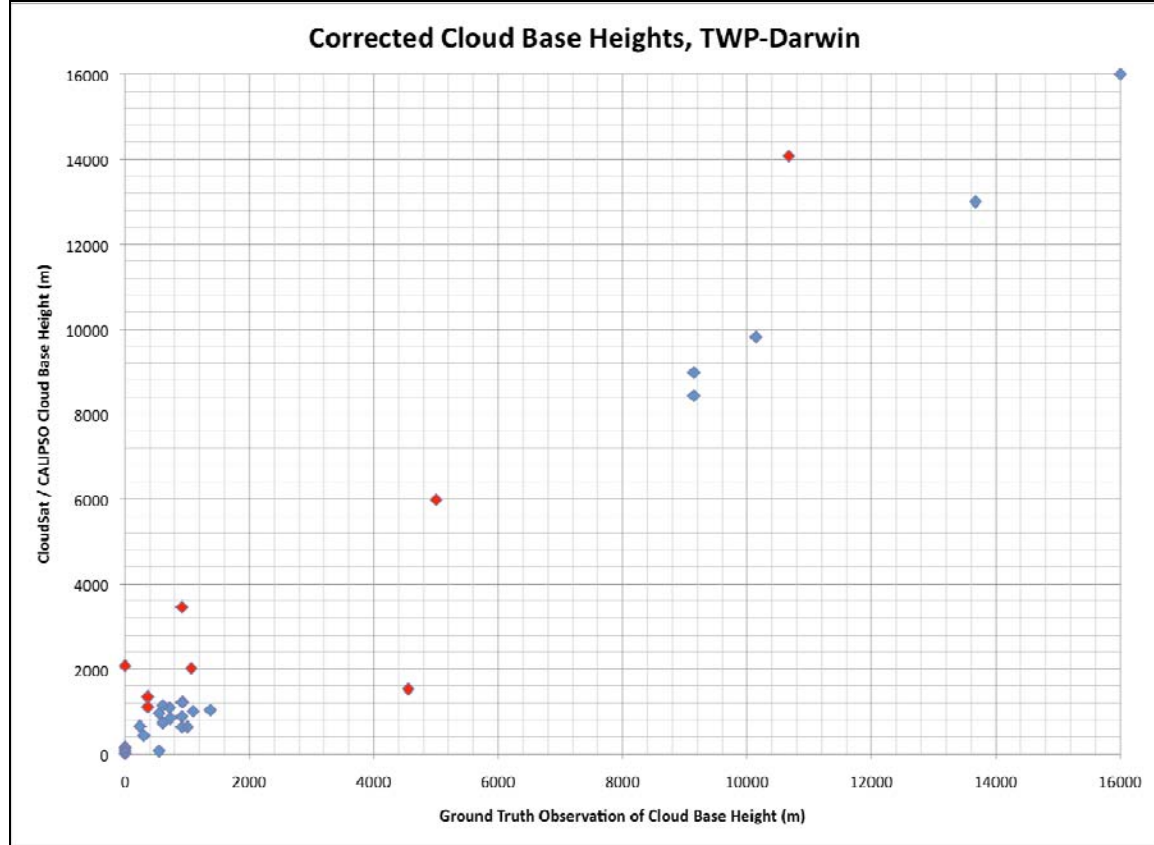
Figure 14.   Initial comparison of CloudSat / CALIPSO 2B-GEOPROF-Lidar cloud base heights versus ground-based assessment of cloud base height for the ARM TWP-Darwin ground site. Red markers denote significant outliers (> 720 m difference).

The TWP-Darwin site was the only site with multiple precipitation events in the data set. Local METAR observations reported precipitation concurrent with the satellite observation on eight occasions. The 2B-GEOPROF-Lidar detection algorithm produced reasonable results in cloud base assessment during these the precipitation events. The original outlier pool for the TWP-Darwin site contained seven of the eight precipitation events. The error in satellite-derived cloud base height in these seven precipitation events averaged 4165 m higher than the ARM cloud base height assessment. However, when compared to local METAR observations, the difference in cloud base heights decreased

to 549 m. This drastic improvement is most likely the result of attenuation of the measurement signals by the falling precipitation for the ARM instruments. In precipitation cases, the human-observed METAR should provide a more accurate value for the cloud base height than the easily attenuated ground-based sensors. Three of the original seven outliers with precipitation were removed from the outlier pool once the METAR confirmed a cloud base height within the accepted 480 m resolution of the satellite-derived cloud base height. The cloud base in six of the eight cases was observed by CloudSat, as the CALIPSO signal completely attenuated in the cloud layer above the falling precipitation. The lidar signal attenuation was most pronounced when CloudSat's cloud classification labeled the hydrometeor layers as "deep convection". Figures 15 and 16 show the total attenuated backscatter from CALIPSO and the radar reflectivity from CloudSat, respectively, for one of the rain events at TWP-Darwin. In the total backscatter plot, the complete attenuation of the lidar signal is evident at approximately 13,400 m, with the VFM placing the cloud base at 13,114 m due to the lack of backscatter data below this level. The total backscatter data reported a maximum backscatter value of 0.0436/km-sr at 14080 m. The radar reflectivity returns from CloudSat showed significant returns (> -20 dBZ) and a corresponding cloud mask value of 40 (complete certainty of cloud presence) to 1531 m, the level reported by the 2B-GEOPROF-Lidar product as the cloud base for the column. The radar reflectivity values remain high (> -23 dBZ) below 1351 m in this case, yet the cloud mask classified the returns as ground clutter rather than as a cloud layer. The combination of CloudSat and CALIPSO data in this case proved useful, but the poor resolution of the hydrometeors in the lowest portion of the column remains a problem for the detection algorithm.
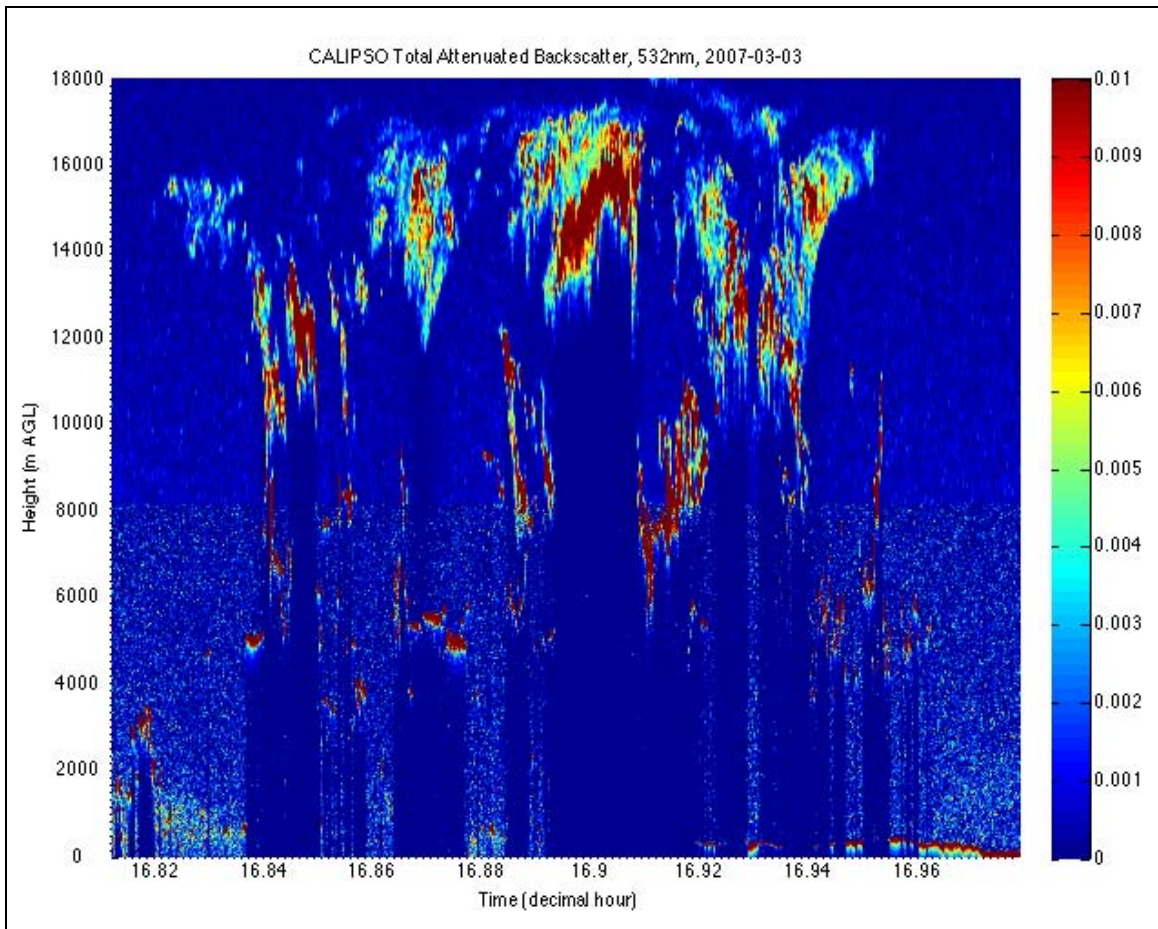
Figure 15.   Total attenuated backscatter recorded by CALIPSO for precipitation event at TWP-Darwin on 3 Mar 2007. CALIPSO's nearest overpass to the ARM ground site occurred at 16.8952 UTC.
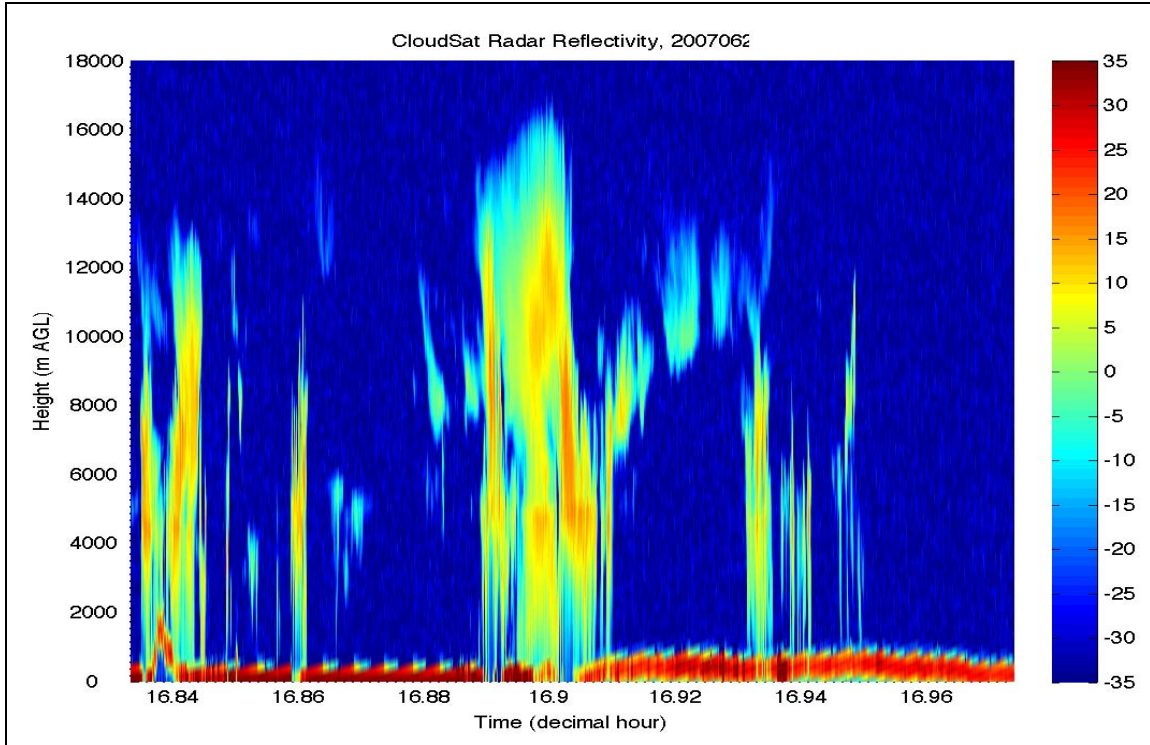
Figure 16.   Radar reflectivity recorded by CloudSat for precipitation event at TWP-
Darwin on 3 Mar 2007. CloudSat's nearest overpass to the ARM ground site
occurred at 16.8904 UTC.

The most problematic mesoscale scenario for cloud base height assessment by
CloudSat and CALIPSO for the TWP-Darwin site was the afternoon sea breeze. Of the
seven data points labeled as significant outliers, MODIS imagery showed cumulus clouds
concentrated along the coast indicative of the afternoon sea breeze in four of these cases.
In three of the cases, the 2B-GEOPROF-Lidar product indicated a CALIPSO-determined
mid-level cloud base in the range of 2000 m to 5900 m, which was 947 m too high, on
average. In each of these cases, CloudSat reported increased radar reflectivity values at
the same levels, but did not label the layer as cloud. Furthermore, the 2B-GEOPROF
Scene Variability reported by CloudSat indicated a "highly variable" profile in these
cases. This means that the cloud element did not fill the complete radar beam and
therefore an accurate assessment of the layer is difficult. The small convective elements
of a sea breeze regime proved to challenge the 2B-GEOPROF-Lidar product and showed
that the cloud base estimates in these carry significant uncertainty.

38

E.   TROPICAL WEST PACIFIC – MANUS RESULTS

The data availability window for the TWP-Manus site was June 21, 2006 to May 23, 2007. The CloudSat and CALIPSO satellite overpass of the TWP-Manus ground site occurred at 0354 UTC (1354 LST) for the satellites' ascending path or 1552 UTC (0152 LST) for the satellites' descending path. The data set for the TWP-Manus location was the smallest of the four sites, with just 30 data points available. The accuracy rate was also the lowest at this location, with the 2B-GEOPROF-Lidar accurately detecting the cloud base height in 18 of the 30 cases (60%). Figure 17 shows the results of the comparison at TWP-Manus.

Due to the orbital mechanics and small ground footprint of CloudSat and CALIPSO, the TWP-Manus geographical location near the equator (-2.006°N, 147.425°E) did not get as many overpasses as the other ARM sites. Because of this, the search window for satellite overpasses was expanded from the 20-km radius around the ARM ground site to a 40-km search radius in order to get a sizable data set, resulting in a average distance between the satellite nadir overpass and the ARM ground site of 39.24 km. This inherently introduced errors in cloud element detection, and coupled with the typical scattered nature clouds in tropical climates, the satellites frequently sampled cloud elements that were not present over the ground site or that were significantly different from the cloud type over the ground site. For samples labeled as outliers, MODIS infrared and visible imagery was inspected to mitigate the impact of sampled clouds that were not reflective of the cloud state over the ground site on the data set's statistics. If the visual inspection revealed that the sampled cloud was in fact not reflective of the cloud state over the ground site, the sample was completely removed from the data set.
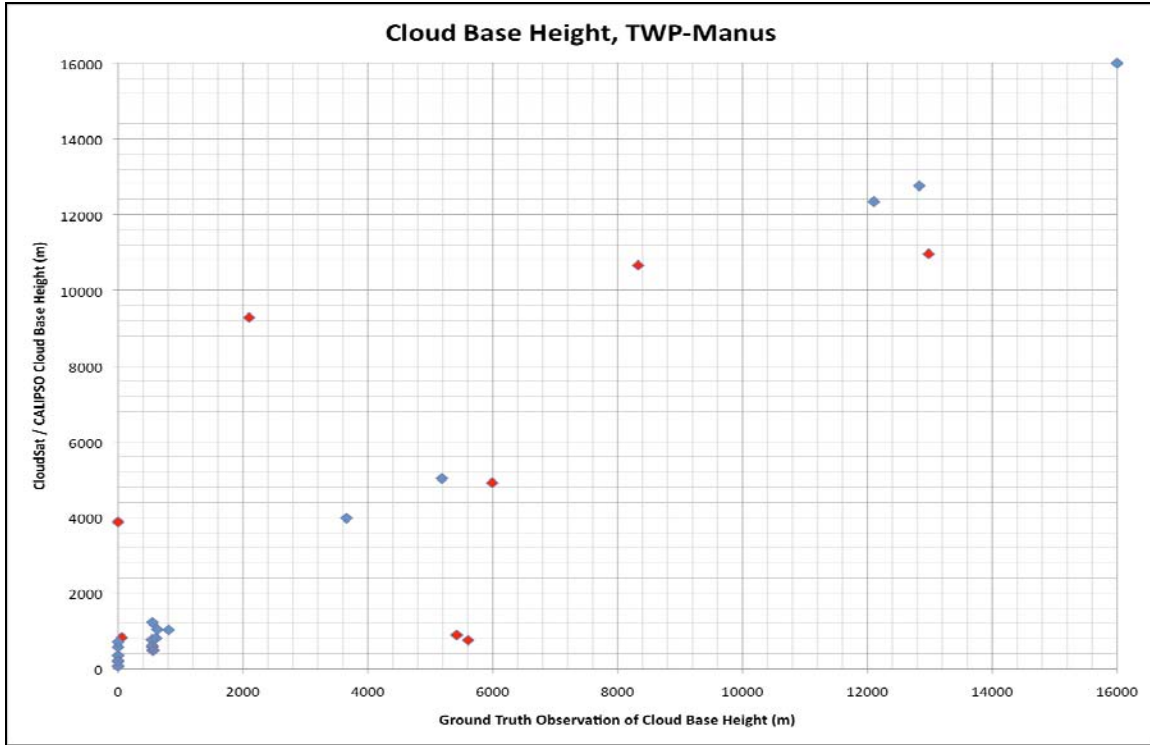
Figure 17.   Comparison of CloudSat / CALIPSO 2B-GEOPROF-Lidar cloud base heights versus ground-based assessment of cloud base height for the ARM TWP-Manus ground site. Red markers denote significant outliers (> 720 m difference).

Another challenge with the TWP-Manus site was the lack of availability of consistently available and useful METAR observations. For the TWP-Manus location, the outlier pool originally contained 20 members. Of these 20 members, only seven had an associated METAR available that provided a cloud observation; the other members either had no observation available, or the observation was automated and did not include a ceilometer reading. Of these seven members with an available cloud observation, five members were removed from the outlier pool since the observed cloud base reported in the METAR was within 480m of the cloud base height recorded in the 2B-GEOPROF-Lidar data. The possibility exists that several of the outliers without a valid METAR cloud base report could actually validate the cloud base height reported by the 2B-GEOPROF-Lidar data; however, without an alternative data source to validate the satellite-measured cloud base height, this is not a safe assumption.

40

V.   SUMMARY AND FUTURE RESEARCH

A.   SUMMARY OF RESEARCH

This thesis study examined the accuracy of cloud base height assessments provided by the 2B-GEOPROF-Lidar data product. This product merged data collected by the CloudSat CPR and the CALIPSO CALIOP to provide a complete assessment of the vertical structure of hydrometeors in an atmospheric column. The cloud base height obtained by the 2B-GEOPROF-Lidar product was compared to cloud base height reported by a suite of ground-based vertically-sampling instruments at four different DOE ARM sites around the globe. These four sites represent distinctly different climatic and geographic areas, thus providing an accurate global assessment of the satellites' capabilities.

For the validation, satellite-observed cloud base heights within 480 m of the cloud base height recorded by the ARM site were accepted as accurate measurements.   Cases where the difference in cloud base height exceeded 480 m were compared against local METAR observations to resolve any potential errors. Cases in which the difference in cloud base height exceeded 720 m were labeled as significant outliers.   The radar reflectivity and cloud mask data from CloudSat and total attenuated backscatter profiles from CALIPSO were examined for the significant outliers. The 2B-GEOPROF-Lidar product provided an accurate assessment of cloud base height in 73% of the 183 cases examined. The average difference between the satellite-derived cloud base height and ground-truth cloud base height was 283 m.

B.   RECOMMENDATIONS FOR FUTURE RESEARCH

Any technology that makes the remote detection of accurate cloud base heights possible is an improvement over current techniques. The combined 2B-GEOPROF-Lidar data from CloudSat and CALIPSO demonstrated that accurate cloud base detection from a space-borne observation platform is now a reality. The key to the success of the data

product lies in the synergistic melding of two different remote sensing techniques to get a complete picture of the atmosphere. Future cloud measurement and monitoring missions should further exploit combined detection methods.

The temporal resolution of this satellite system is a considerable drawback for real time operational use. Unfortunately the only way to resolve this problem is to launch more satellites--an expensive proposition. The data collected by CloudSat and CALIPSO can still provide valuable insights for improved cloud forecasts. The ability to gather cloud height data in areas previously left to rudimentary interpolation must be appealing to the modeling community. Long term studies of cloud trends and behaviors in high interest regions of the world based on data from CloudSat and CALIPSO could drastically improve cloud analysis algorithms like those used by the Air Force Weather Agency (AFWA) in the Cloud Depiction and Forecast System (CDFS-II). Improvements to the CDFS-II algorithms could drastically improve the accuracy and effectiveness of AFWA's operational World Wide Merged Cloud Analysis (WWMCA) (Air Force Weather Agency 2007).

Improvements to the detection algorithms of each instrument can further increase the viability of remote cloud base height assessments as a valuable meteorological analysis and forecasting tool. This research showed a clear bias towards classifying hydrometeors detected in the lowest 500 m of the column as ground clutter. By ignoring this low-level feature, the algorithm consistently placed the cloud base too high since it defaulted to the next higher significant layer above the low-level feature. Fine-tuning of the CPR SEM could improve this consistent error. Special care must be taken to ensure that the sensitivity to hydrometeors in the upper levels is not impacted when increasing sensitivity in the low-levels. The development of a separate detection algorithm specifically designed to resolve hydrometeors in the lowest levels of the column could isolate the problematic layers, possibly reducing the number of low-level cloud layers incorrectly classified as ground clutter. However, the 480 m resolution of the CPR will always limit these improvements.

LIST OF REFERENCES

Air Force Weather Agency, 2007: Algorithm Description for the Cloud Depiction and Forecast System II. HQ AFWA / A8TM, Offutt AFB, NE.

Baedi, R., R. Boers, and H. Russchenberg, 2002: Detection of Boundary Layer Water Clouds by Spaceborne Cloud Radar. *J. Atmos. Oceanic Technol.,* **19**, 1915-1927.

Clothiaux, E. E., M. A. Miller, B. A. Albrecht, T. P. Ackerman, J. Verlinde, D. M. Babb, R. M. Peters, and W. J. Syrett, 1995: An Evaluation of a 94-GHz Radar for Remote Sensing of Cloud Properties. *J. Atmos. Oceanic Technol.,* **12**, 201-229.

Clothiaux, G. G. Mace, and T. P. Ackerman, 1998: An Automated Algorithm for Detection of Hydrometeor Returns in Micropulse Lidar Data. *J. Atmos. Oceanic Technol.,* **15**, 1035-1042.

Clothiaux, E. E., T. P. Ackerman, G. G. Mace, K. P. Moran, R. T. Marchand, M. A. Miller, and B. E. Martner, 2000: Objective Determination of Cloud Heights and Radar Reflectivities Using a Combination of Active Remote Sensors at the ARM CART Sites. *J. Appl. Meteor.,* **39**, 645-665.

Cooperative Institute for Research in the Atmosphere, 2007: CloudSat Standard Data Products Handbook. 19 pp. [Available online at http://www.cloudsat.cira.colostate.edu/cloudsat_documentation/CloudSat_Data_Users_Handbook.pdf.]

Forsythe, J. M., T. H. Vonder Haar, and D. L. Reinke, 2000: Cloud-Base Height Estimates Using a Combination of Meteorological Satellite Imagery and Surface Reports. *J. Appl. Meteor.,* **39**, 2336-2347.

Goddard Space Flight Center, 2003: Formation Flying: The Afternoon "A-Train" Satellite Constellation. *NASA Facts: The Earth Science Enterprise Series,* FS-2003-1-053-GSFC. 6 pp. [Available online at aqua.nasa.gov/doc/pubs/A-Train_Fact_sheet.pdf.]

Lhermitte, R. M., 1988: Cloud and Precipitation Remote Sensing at 94 GHz. *IEEE Trans. Geosci. Remote Sens.,* **26**, 207-216.

Liu, Z., A. H. Omar, Y. Hu, M. A. Vaughan, and D. M. Winker, 2005: CALIOP Algorithm Theoretical Basis Document Part 3: Scene Classification Algorithms. 56 pp.

Mace, G. G., R. Marchand, Q. Zhang, and G. L. Stephens, 2007a: Global hydrometeor occurrence as observed by CloudSat: Initial observations from summer 2006. *Geophys. Res. Lett.,* **34**, 5 pp, doi:10.1029/2006GL029017.

Mace, G., D. Vane, G. Stephens, and D. Reinke, 2007b: Level 2 Radar-Lidar GEOPROF Product Version 1.0 Process Description and Interface Control Document, 19 pp. [Available online at http://www.cloudsat.cira.colostate.edu/dataICDlist.php?go =list&path=/2B-GEOPROF-LIDAR.]

Mace, G., 2007: Level 2 GEOPROF Product Process Description and Interface Control Document Algorithm, Version 5.3, 43 pp. [Available online at http://www.cloudsat.cira.colostate.edu/dataICDlist.php?go=list&path=/2B-GEOPROF.]

Marchand, R., J. Mace, and Q. Zhang, 2007: 2B-GEOPROF Interface Control Document, Version 5.3. 26 pp. [Available online at http://www.cloudsat.cira.colostate.edu/ icd_pdf.php?avid=98&pvids=191.]

Marchand, R., G. G. Mace, T. Ackerman, and G. Stephens, 2008: Hydrometeor Detection Using *CloudSat*--An Earth-Orbiting 94-GHz Cloud Radar. *J. Atmos. Oceanic Technol.,* **25**, 519-533, doi:10.1175/2007JTECHA1006.1.

Stephens, G. L. and Coauthors, 2002: The CloudSat Mission and the A-Train: A New Dimension of Space-Based Observations of Cloud and Precipitation. *Bull. Amer. Meteor. Soc.,* **83**, 1771-1790.

Vaughan, M. A., D. M. Winker, and C. A. Hostetler, 2002: "SIBYL: a selective iterated boundary location algorithm for finding cloud and aerosol layers in CALIPSO lidar data", in *Lidar Remote Sensing in Atmos. and Earth Sci.,* L. R. Bissonnette, G. Roy and G. Vallée (editors), Defence R&D Canada - Valcartier, Québec, Canada, 791-794.

Vaughan, M., S. Young, D. Winker, K. Powell, A. Omar, Z. Liu, Y. Hu, and C. Hostetler, 2004: Fully automated analysis of space-based lidar data: an overview of the CALIPSO retrieval algorithms and data products. *Proc. of SPIE,* **5575**, 16-30, doi:10.1117/12.572024.

Wang, Z., K. Sassen, 2007: Level 2 Cloud Scenario Classification Product Process Description and Interface Control Document, Version 5.0, 50 pp. [Available online at http://www.cloudsat.cira.colostate.edu/dataICDlist.php?go=list& path=/2B-CLDCLASS.]

Winker, D. M., 2006: The CALIPSO Mission and Initial Observations of Aerosols and Clouds from CALIOP. *Proc. SPIE,* **6409**, 3 pp.

Winker, D. M., R. H. Couch, and M. P. McCormick, 1996: An Overview of LITE: NASA's Lidar In-space Technology Experiment. *IEEE,* **84**, 164-180.

Winker, D. M., C. A. Hostetler, M. A. Vaughan, and A. H. Omar, 2006: CALIOP Algorithm Theoretical Basis Document Part 1: CALIOP Instrument and Algorithms Overview, Release 2.0. 29 pp. [Available online at http://www-calipso.larc.nasa.gov/resources/pdfs/PC-SCI-202.Part1_v2-Overview.pdf.]

Winker, D. M., W. Hunt, and C. Hostetler, 2004: Status and performance of the CALIOP lidar. *Proc. SPIE,* **5575**, 8 pp.

Winker, D. M., J. Pelon, and M. P. McCormick, 2003: The CALIPSO mission: Spaceborne lidar for observation of aerosols and clouds. *Proc. SPIE,* **4893**, 11 pp.

THIS PAGE INTENTIONALLY LEFT BLANK

INITIAL DISTRIBUTION LIST

1. Defense Technical Information Center
   Ft. Belvoir, Virginia

2. Dudley Knox Library
   Naval Postgraduate School
   Monterey, California

3. Air Force Weather Technical Library
   Asheville, North Carolina